DYNAMIC STABILITY DERIVATIVES OF A TWIN-JET FIGHTER MODEL FOR ANGLES OF ATTACK FROM -10° TO 110°

by Sue B. Grafton and Charles E. Libbey

Langley Research Center
Hampton, Va. 23365

NATIONAL AERONAUTICS AND SPACE ADMINISTRATION • WASHINGTON, D. C. • JANUARY 1971

1. Report No.	2. Government Accession No.	3. Recipient's Catalog No.
NASA TN D-6091		

4. Title and Subtitle
DYNAMIC STABILITY DERIVATIVES OF A TWIN-JET FIGHTER MODEL FOR ANGLES OF ATTACK FROM -10° TO 110°

5. Report Date
January 1971

6. Performing Organization Code

7. Author(s)
Sue B. Grafton and Charles E. Libbey

8. Performing Organization Report No.
L-7370

9. Performing Organization Name and Address
NASA Langley Research Center
Hampton, Va. 23365

10. Work Unit No.
126-63-11-36

11. Contract or Grant No.

12. Sponsoring Agency Name and Address
National Aeronautics and Space Administration
Washington, D.C. 20546

13. Type of Report and Period Covered
Technical Note

14. Sponsoring Agency Code

15. Supplementary Notes

16. Abstract

A low-speed investigation was conducted to determine the dynamic stability derivatives in pitch, roll, and yaw over an angle-of-attack range of -10° to 110° for a twin-jet swept-wing fighter model. Several frequencies and amplitudes were investigated to determine the effects of these variables on the stability derivatives. The effect of the vertical and horizontal tail, and horizontal-tail incidence on the derivatives was also evaluated. The results indicate that the model exhibited stable values of damping in pitch over the entire angle-of-attack range, but marked reductions of damping in roll were measured at the stall, and unstable values of damping in yaw were present for the very high angles of attack associated with flat spins. Either removal of the horizontal or vertical tail or full up deflection of the horizontal tail eliminated the unstable characteristics of the damping-in-yaw derivatives.

17. Key Words (Suggested by Author(s))	18. Distribution Statement
Dynamic derivatives Fighter airplane	Unclassified – Unlimited

19. Security Classif. (of this report)	20. Security Classif. (of this page)	21. No. of Pages	22. Price*
Unclassified	Unclassified	36	$3.00

*For sale by the National Technical Information Service, Springfield, Virginia 22151

DYNAMIC STABILITY DERIVATIVES OF A TWIN-JET FIGHTER MODEL FOR ANGLES OF ATTACK FROM -10° TO 110°

By Sue B. Grafton and Charles E. Libbey
Langley Research Center

SUMMARY

A low-speed investigation was conducted in the Langley full-scale tunnel to determine the dynamic stability derivatives in pitch, roll, and yaw over an angle-of-attack range of -10° to 110° for a twin-jet swept-wing fighter airplane. The study consisted of forced-oscillation tests of a 0.13-scale model of the airplane at a Reynolds number of 1.33×10^6. Several oscillatory frequencies and amplitudes were investigated to determine the effects of these variables on the stability derivatives. The effects of the vertical and horizontal tail, and of the horizontal-tail deflection, on the derivatives were also evaluated.

The results of the investigation indicated that the model exhibited stable values of damping in pitch over the entire angle-of-attack range, but marked reductions of damping in roll were measured at the stall, and unstable values of damping in yaw were present for the very high angles of attack associated with flat spins. These unstable values of damping in yaw, which constitute propelling moments in a spin, were produced by aerodynamic interference between the vertical and horizontal tails. Either removal of the horizontal or vertical tail or full up deflection of the horizontal tail eliminated the propelling moments.

INTRODUCTION

The National Aeronautics and Space Administration is currently engaged in a research program to develop and validate theoretical methods for prediction of airplane stall and spin characteristics. A major portion of this program involves correlation between theoretical calculations and data obtained by free-flight tests using dynamically scaled radio-controlled models of fighter airplanes. Previous theoretical and experimental results obtained for a variable-sweep fighter with a long pointed nose are reported in reference 1.

The present investigation was conducted to measure the dynamic stability derivatives of a twin-jet swept-wing fighter model over the angle-of-attack range associated with spinning; these data are intended to serve as aerodynamic input for additional

theoretical studies of the stall and spin characteristics of this particular configuration. The investigation consisted of forced-oscillation tests which were conducted over an angle-of-attack range from -10° to 110° and included the effects of frequency and amplitude of the oscillatory motion. Tests were also conducted with the vertical and horizontal tails removed. The effect of horizontal-tail deflection on the yawing dynamic derivatives is also presented. Pertinent static force tests were conducted to aid in the analysis of the dynamic data.

SYMBOLS

Physical Concepts

The longitudinal and lateral-directional data presented herein are referred to the body-axis system (see fig. 1). All data are referred to a center-of-gravity position of 33-percent mean aerodynamic chord.

In order to facilitate international usage of data presented, dimensional quantities are presented both in the U.S. Customary Units and in the International System of Units (SI). Equivalent dimensions were determined by using the conversion factors given in reference 2.

b	wing span, ft (m)
$\bar{c}$	mean aerodynamic chord, ft (m)
$\bar{c}_h$	mean aerodynamic chord of horizontal tail, ft (m)
F_A	force along X body axis, lb (N)
F_Y	force along Y body axis, lb (N)
F_N	force along Z body axis, lb (N)
f	frequency of oscillation, cycles/sec
k	reduced-frequency parameter, $\frac{\omega b}{2V}$ for lateral-directional parameter or $\frac{\omega \bar{c}}{2V}$ for longitudinal parameter
M_X	rolling moment, ft-lb (m-N)

M_Y	pitching moment, ft-lb (m-N)
M_Z	yawing moment, ft-lb (m-N)
p	rolling velocity, rad/sec
q	pitching velocity, rad/sec
q_∞	free-stream dynamic pressure, $\frac{\rho V^2}{2}$, lb/ft^2 (N/m^2)
r	yawing velocity, rad/sec
S	wing area, ft^2 (m^2)
u,v,w	components of resultant velocity V_A along X, Y, and Z body axes, respectively, ft/sec (m/sec)
V	free-stream velocity, ft/sec (m/sec)
V_A	resultant linear velocity, ft/sec (m/sec)
X,Y,Z	body reference axes
α	angle of attack, deg or rad
β	angle of sideslip, deg or rad
δ_h	horizontal-tail deflection, positive when trailing edge down, deg
ρ	air density, $slugs/ft^3$ (kg/m^3)
θ	angle of pitch, deg or rad
$\Delta\theta$	pitch-angle increment, deg
ϕ	angle of roll, deg or rad
$\Delta\phi$	roll-angle increment, deg

ψ angle of yaw, deg or rad

$\Delta\psi$ yaw-angle increment, deg

ω angular velocity, $2\pi f$, rad/sec

Dot over symbol indicates derivative with respect to time.

Coefficients and Derivatives

Results presented herein are given in terms of the coefficients and derivatives defined in the tabulations that follow:

Normal force	Axial force	Pitching moment
$C_N = \frac{F_N}{q_\infty S}$	$C_A = \frac{F_A}{q_\infty S}$	$C_m = \frac{M_Y}{q_\infty S\bar{c}}$
$C_{N_\alpha} = \frac{\partial C_N}{\partial \alpha}$	$C_{A_\alpha} = \frac{\partial C_A}{\partial \alpha}$	$C_{m_\alpha} = \frac{\partial C_m}{\partial \alpha}$
$C_{N_q} = \frac{\partial C_N}{\partial \frac{q\bar{c}}{2V}}$	$C_{A_q} = \frac{\partial C_A}{\partial \frac{q\bar{c}}{2V}}$	$C_{m_q} = \frac{\partial C_m}{\partial \frac{q\bar{c}}{2V}}$
$C_{N_{\dot\alpha}} = \frac{\partial C_N}{\partial \frac{\dot\alpha\bar{c}}{2V}}$	$C_{A_{\dot\alpha}} = \frac{\partial C_A}{\partial \frac{\dot\alpha\bar{c}}{2V}}$	$C_{m_{\dot\alpha}} = \frac{\partial C_m}{\partial \frac{\dot\alpha\bar{c}}{2V}}$
$C_{N_{\dot q}} = \frac{\partial C_N}{\partial \frac{\dot q\bar{c}}{4V^2}}$	$C_{A_{\dot q}} = \frac{\partial C_A}{\partial \frac{\dot q\bar{c}}{4V^2}}$	$C_{m_{\dot q}} = \frac{\partial C_m}{\partial \frac{\dot q\bar{c}}{4V^2}}$

Rolling moment	Yawing moment	Side force
$C_l = \frac{M_X}{q_\infty Sb}$	$C_n = \frac{M_Z}{q_\infty Sb}$	$C_Y = \frac{F_Y}{q_\infty S}$
$C_{l_p} = \frac{\partial C_l}{\partial \frac{pb}{2V}}$	$C_{n_p} = \frac{\partial C_n}{\partial \frac{pb}{2V}}$	$C_{Y_p} = \frac{\partial C_Y}{\partial \frac{pb}{2V}}$
$C_{l_r} = \frac{\partial C_l}{\partial \frac{rb}{2V}}$	$C_{n_r} = \frac{\partial C_n}{\partial \frac{rb}{2V}}$	$C_{Y_r} = \frac{\partial C_Y}{\partial \frac{rb}{2V}}$
$C_{l_\beta} = \frac{\partial C_l}{\partial \beta}$	$C_{n_\beta} = \frac{\partial C_n}{\partial \beta}$	$C_{Y_\beta} = \frac{\partial C_Y}{\partial \beta}$
$C_{l_{\dot\beta}} = \frac{\partial C_l}{\partial \frac{\dot\beta b}{2V}}$	$C_{n_{\dot\beta}} = \frac{\partial C_n}{\partial \frac{\dot\beta b}{2V}}$	$C_{Y_{\dot\beta}} = \frac{\partial C_Y}{\partial \frac{\dot\beta b}{2V}}$
$C_{l_{\dot p}} = \frac{\partial C_l}{\partial \frac{\dot p b^2}{4V^2}}$	$C_{n_{\dot p}} = \frac{\partial C_n}{\partial \frac{\dot p b^2}{4V^2}}$	$C_{Y_{\dot p}} = \frac{\partial C_Y}{\partial \frac{\dot p b^2}{4V^2}}$
$C_{l_{\dot r}} = \frac{\partial C_l}{\partial \frac{\dot r b^2}{4V^2}}$	$C_{n_{\dot r}} = \frac{\partial C_n}{\partial \frac{\dot r b^2}{4V^2}}$	$C_{Y_{\dot r}} = \frac{\partial C_Y}{\partial \frac{\dot r b^2}{4V^2}}$

In the present investigation the term "in-phase derivative" refers to any one of the oscillatory derivatives that is based on the components of forces and moments in phase with the angle of pitch, roll, or yaw produced in the oscillatory tests. The term "out-of-phase derivative" refers to any one of the oscillatory derivatives that is based on the

components of forces and moments 90° out of phase with the angle of pitch, roll, or yaw. The oscillatory derivatives of the present investigation were measured in the following combinations:

In phase	Out of phase
Pitching	
$C_{m_\alpha} - k^2 C_{m_{\dot{q}}}$	$C_{m_q} + C_{m_{\dot{\alpha}}}$
$C_{N_\alpha} - k^2 C_{N_{\dot{q}}}$	$C_{N_q} + C_{N_{\dot{\alpha}}}$
$C_{A_\alpha} - k^2 C_{A_{\dot{q}}}$	$C_{A_q} + C_{A_{\dot{\alpha}}}$
Rolling	
$C_{Y_\beta} \sin \alpha - k^2 C_{Y_{\dot{p}}}$	$C_{Y_p} + C_{Y_{\dot{\beta}}} \sin \alpha$
$C_{n_\beta} \sin \alpha - k^2 C_{n_{\dot{p}}}$	$C_{n_p} + C_{n_{\dot{\beta}}} \sin \alpha$
$C_{l_\beta} \sin \alpha - k^2 C_{l_{\dot{p}}}$	$C_{l_p} + C_{l_{\dot{\beta}}} \sin \alpha$
Yawing	
$C_{Y_\beta} \cos \alpha + k^2 C_{Y_{\dot{r}}}$	$C_{Y_r} - C_{Y_{\dot{\beta}}} \cos \alpha$
$C_{n_\beta} \cos \alpha + k^2 C_{n_{\dot{r}}}$	$C_{n_r} - C_{n_{\dot{\beta}}} \cos \alpha$
$C_{l_\beta} \cos \alpha + k^2 C_{l_{\dot{r}}}$	$C_{l_r} - C_{l_{\dot{\beta}}} \cos \alpha$

APPARATUS AND MODEL

Wind Tunnel

The tests were made in the 30- by 60-foot (9.1- by 18.3-m) open-throat test section of the Langley full-scale tunnel with the model mounted about 10 feet (3.05 m) above the groundboard with its wings in a vertical plane. The model was so small in proportion to the tunnel test section that no wind-tunnel jet-boundary or blockage corrections were required.

Model

The investigation was conducted with a 0.13-scale model of a two-place twin-jet high-performance fighter designed for land and carrier-based operations. A three-view sketch showing the general layout of the model is presented in figure 2; a photograph of the model is shown in figure 3, and geometric characteristics of the full-scale airplane are listed in table I. The longitudinal-control system of the configuration consists of an all-movable horizontal tail which incorporates negative dihedral of 23° to satisfy the longitudinal stability requirements in the normal operational flight range. Lateral control is provided by spoilers as well as ailerons. The ailerons deflect downward while the spoilers deflect upward. The left aileron and right spoiler operate simultaneously as do the right aileron and left spoiler. The directional-control system consists of a conventional rudder. The maximum control-surface deflections are as follows:

Rudder deflection, deg	± 30
Horizontal-tail deflection (trailing edge), deg	21 up, 9 down
Aileron deflection, deg	0 up, 30 down
Spoiler deflection, deg	45 up, 0 down

All dynamic force tests were made with a single-strut support system and an internal six-component strain-gage balance. The test setups for pitching, rolling, and yawing are illustrated in figure 4 and the equipment and readout system is described in reference 3. The model and the strain-gage balance were mounted on the oscillation sting assembly so that the moment reference center of the balance was at the center-of-gravity location shown in figure 2 (33 percent $\bar{c}$) and was on the axis of rotation for all test conditions. Oscillatory motion was imparted to the model by means of a flywheel that was driven by a 3-horsepower (2.2-kilowatt) variable-speed electric motor and a system of pushrods and bellcranks. The amplitude of the oscillatory motion was adjusted by varying the location of the lower pivot point of the vertical connecting rod along the radius of the flywheel. The frequency of the oscillatory motion (limited to about 2 cycles per second) was varied by changing the speed of the electric motor.

A precision sine-cosine potentiometer, which generated voltage signals proportional to the sine and cosine of the flywheel rotation angle, was coupled directly to the flywheel shaft and provided electrical signals proportional to the angular displacement of the model. These signals were used in the data readout procedure described in detail in reference 3.

TESTS

The forced-oscillation tests in pitch, roll, and yaw were conducted over an angle-of-attack range from -10° to 110°. The tests were conducted in the Langley full-scale tunnel

at a speed of 100 feet per second (30.48 m/sec) which corresponds to a Reynolds number of about 1.33×10^6 based on the mean aerodynamic chord of the wing. Tests were made for the complete model and also for the model with the horizontal or vertical tails individually removed, and with the horizontal tails deflected to -21°. The tests were conducted for amplitudes ranging from $\pm 2.47^\circ$ to $\pm 10.5^\circ$ and at frequencies of 0.5, 0.7, 1.0, and 1.3 and 1.5 cycles per second over the entire angle-of-attack range.

RESULTS AND DISCUSSION

The more pertinent results with regard to stall and spin characteristics have been reviewed in previous reports. Lateral-directional characteristics of this airplane at the stall have been reported in reference 4 while aerodynamic factors affecting flat spin tendencies are presented in reference 5. The results presented herein, which form a complete documentation of dynamic stability derivatives at low speed, are therefore presented with a minimum amount of analysis.

Static Aerodynamic Characteristics

Longitudinal characteristics.- The static longitudinal characteristics of the model as functions of angle of attack are presented in figure 5. Results are shown for horizontal-tail deflection angles of 0° and -21° (corresponding to stick full back), and also for the horizontal-tail-off condition. The normal-force coefficients presented in figure 5(a) indicate that significant flow separation and stall began to appear at an angle of attack of about 12°. The variation of the axial-force coefficient shown in figure 5(b) also indicates onset of flow separation at about 12°. The results presented in figure 5(c) indicate that the model is statically unstable over a small angle-of-attack range just at the onset of the stall (12° to 18°), but has control effectiveness sufficient to overcome any pitchup or deep-stall trim condition. With the stick full back $(\delta_h = -21^\circ)$, the model can be trimmed at an angle of attack well above the stall, and the model is statically stable at all elevator positions throughout the spin angle-of-attack region. Above the stall, pitch-control effectiveness decreases to a minimum at about $\alpha = 60^\circ$ but then increases as angle of attack approaches 90°. The results obtained with the horizontal tail off indicate that the horizontal tails contribute a very large diving moment in the spin angle-of-attack region. These results also reveal that the small region of static instability near the stall is also present with the horizontal tail off and is apparently related to wing stall.

Lateral-directional characteristics.- The static lateral-directional stability derivatives of the model are presented in figure 6 as functions of angle of attack based on values of the coefficients at $\beta = \pm 5^\circ$. Results are shown for horizontal-tail deflections of 0°, -21°, and (over a limited angle-of-attack range) for the horizontal-tail-off condition. These results indicate that the model is directionally stable up to angles of attack slightly

above the stall (about 21°) and that effective dihedral increases about linearly with angle of attack up to $\alpha = 12^{\circ}$, where flow separation begins, and causes a marked reduction in C_{l_β} until it becomes zero at about the same angle of attack at which the model becomes directionally unstable. This combination of directional instability and zero effective dihedral at angle of attack in the region just beyond the stall is conducive to directional divergence problems which might lead to an inadvertent spin entry. Reference 4 discusses the factors which cause the directional divergence to occur for this airplane configuration. The results of reference 4 indicated that loss of directional stability resulted from a combination of an adverse sidewash region at the rear of the model and a reduction in dynamic pressure at the vertical-tail location.

For the angle-of-attack range above 40° the model with controls neutral $(\delta_h = 0^{\circ})$ remained directionally unstable. Deflection of the horizontal tail to the full-back-stick condition $(\delta_h = -21^{\circ})$ caused the directional instability above the stall to be more severe up to angles of attack of about 60°, and again at angles of attack above 88°. This result indicates the probability of an interference effect between the horizontal and vertical tails at these angles of attack. The model had positive effective dihedral for the entire angle-of-attack range above $\alpha = 40^{\circ}$ and C_{l_β} was not appreciably affected by deflection or removal of the horizontal tail in the angle-of-attack range. A discussion of the significance of the aerodynamic characteristics at very high angles of attack in terms of the flat spin is given in reference 5.

Dynamic Stability Derivatives

Pitching.- Comparisons of the effects of amplitude and frequency on the out-of-phase and in-phase pitching derivatives are presented in figures 7 and 8, respectively, for a limited angle-of-attack range (-7° to 28°). The out-of-phase pitching derivatives for the two largest amplitudes tested are presented in figure 9 for the entire angle-of-attack range investigated (-12° to 108°).

The results presented in figures 7 and 8 indicate that damping-in-pitch increases in the α-range where static instability occurred (12.5° to 17.5°) in that the derivative combination $C_{m_q} + C_{m_{\dot{\alpha}}}$ became more negative. This result is probably related to flow separation on the wing. The effect of removal of the horizontal tails was to reduce $C_{m_q} + C_{m_{\dot{\alpha}}}$ in the low angle-of-attack range, but this increment was gradually reduced above the stall. The in-phase derivative $\left(C_{m_\alpha} - k^2 C_{m_{\dot{q}}}\right)$ reflects the trend of the static data; that is, the model exhibited reduced stability for 12° to 18° and this reduction was caused by the wing-fuselage combination. Figure 9 shows that the horizontal tail provides more than half of the pitch damping over all but a small range of angle of attack between 30° and 33°. In this angle-of-attack range the horizontal tail is probably in the low dynamic pressure stalled wake of the wing. At the larger amplitude of oscillation

this effect is less pronounced as would be expected because at either end of the oscillation the horizontal tail leaves the stalled wake effects of the wing.

There appear to be no appreciable frequency effects on $C_{m_q} + C_{m_{\dot{\alpha}}}$ up to an angle of attack of 28° as shown in figure 7; increasing the angle of attack beyond approximately 28° as shown in figure 9 resulted in no consistent trend in the frequency effects on this out-of-phase derivative. For the in-phase derivative, $C_{m_\alpha} - k^2 C_{m_{\dot{q}}}$ (fig. 8), increasing the frequency generally caused this derivative to become more stable, and these effects were most pronounced in the angle-of-attack range where static instability had been shown to occur. This result is probably related to the well-known fact that flow separation is delayed by increased frequency.

The effects of increasing pitch amplitude are mainly smoothing effects, as would be expected, because the nonlinearities in the data would tend to be averaged out with larger amplitude motions. Thus, the sharp peaks in both the out-of-phase and in-phase data at low amplitudes are flattened out as amplitude is increased (figs. 7, 8, and 9). No consistent trends were observed in the out-of-phase normal-force derivatives at all amplitudes and frequencies, and, consequently, no positive comments as to the effects of amplitude or frequency can be offered. (See figs. 7 and 9.) The in-phase normal-force derivatives (fig. 8) were very consistent in that the effects of increasing frequency were to increase $C_{N_\alpha} - k^2 C_{N_{\dot{q}}}$ in the separated flow region. Essentially no effects of frequency occurred on either the in-phase or out-of-phase axial-force derivatives. Since there was no appreciable effect of frequency on either the out-of-phase or in-phase pitching derivatives, the data in figure 9 are faired only for the midfrequency range in order to present a clear picture of the contribution of the horizontal tail.

Rolling.- The effects of frequency and amplitude on the out-of-phase and in-phase rolling derivatives over the angle-of-attack range of -8° to 112° are presented in figures 10 and 11, respectively.

The damping in roll $\left(C_{l_p} + C_{l_{\dot{\beta}}} \sin \alpha\right)$ decreases significantly in the stall range and at the low oscillation frequencies becomes unstable. This marked reduction of damping in roll at the stall is believed to be the basic factor producing lightly damped lateral oscillations or "wing rock" at high angles of attack as discussed in reference 4. As can be seen, the magnitude and sense of damping in roll is a strong function of both amplitude and frequency near the stall. As pointed out in reference 4, reduced damping in roll will result in a lightly damped Dutch roll motion. Extremely large positive values of $C_{n_p} + C_{n_{\dot{\beta}}} \sin \alpha$ (fig. 10) were experienced in the flat spin range ($\alpha = 80^\circ$ to 90°). Neither the source nor significance of these large moments is known.

Yawing.- The out-of-phase yawing derivatives for three frequencies and two amplitudes for angles of attack of -12° to 108° are presented in figure 12 for the complete model. These data indicate that neither frequency nor amplitude had any significant

effect in the unstalled angle-of-attack range, but at higher angles of attack (α greater than about 20°) there were considerable effects of these factors, especially in $C_{n_r} - C_{n_{\dot{\beta}}} \cos \alpha$ and $C_{Y_r} - C_{Y_{\dot{\beta}}} \cos \alpha$. The model has stable damping in yaw (negative values of $C_{n_r} - C_{n_{\dot{\beta}}} \cos \alpha$) through most of the angle-of-attack range, but at spinning angles of attack of 60° and greater the model has unstable or positive values of damping in yaw. These positive values are an indication that propelling or autorotational yawing moments are present on the model, and their effect on the flat spin is discussed in reference 5. Figure 13 shows the contributions of the horizontal and vertical tails to both the out-of-phase and in-phase yawing derivatives. The vertical tail begins to lose its effectiveness at an angle of attack of about 25°. The vertical- and horizontal-tail combination becomes effective again, in an adverse sense, in the flat spin range (α between 70° and 90°) and produces large propelling moments. Removing only the horizontal tail completely eliminates the unstable condition and removing only the vertical tail eliminates the condition at angles of attack above 75°. The unstable condition is caused by aerodynamic interference between the horizontal tail and the vertical tail. This phenomenon is explained and illustrated with smoke flow studies in reference 5. Inasmuch as the propelling moments were known to be caused by interference between the vertical and horizontal tail and previous studies had shown large effects of horizontal-tail deflection angle on these moments, additional tests were conducted to determine the effect of δ_h on $C_{n_r} - C_{n_{\dot{\beta}}} \cos \alpha$. The results of these tests are presented in figure 14. In the flat spin range of 80° to 90° angle of attack the full-up elevator deflection changed $C_{n_r} - C_{n_{\dot{\beta}}} \cos \alpha$ from propelling to damping, although it is less effective than removing the horizontal tails completely. At angles of attack above 95° this combination produced unstable damping in yaw.

CONCLUDING REMARKS

As a result of the analysis of the oscillatory dynamic stability derivatives of the model over an angle-of-attack range of -10° to 110° and at a Reynolds number of 1.33×10^6, the following significant points are noted:

1. The model exhibited stable damping in pitch over the angle-of-attack range investigated, but marked reductions in damping in roll were measured at the stall and unstable values of damping in yaw were measured at angles of attack associated with flat spins.

2. The model had unstable values of damping in yaw. These values constitute propelling moments in a spin and were produced by aerodynamic interference between the

vertical and horizontal tails. Either removal of the horizontal or vertical tail or full up deflection of the horizontal tail eliminated the propelling moments.

Langley Research Center,
National Aeronautics and Space Administration,
Hampton, Va., September 25, 1970.

REFERENCES

1. Chambers, Joseph R.; Anglin, Ernie L.; and Bowman, James S., Jr.: Effects of a Pointed Nose on Spin Characteristics of a Fighter Airplane Model Including Correlation With Theoretical Calculations. NASA TN D-5921, 1970.

2. Mechtly, E. A.: The International System of Units – Physical Constants and Conversion Factors. NASA SP-7012, 1964.

3. Chambers, Joseph R.; and Grafton, Sue B.: Static and Dynamic Longitudinal Stability Derivatives of a Powered 1/9-Scale Model of a Tilt-Wing V/STOL Transport. NASA TN D-3591, 1966.

4. Chambers, Joseph R.; and Anglin, Ernie L.: Analysis of Lateral-Directional Stability Characteristics of a Twin-Jet Fighter Airplane at High Angles of Attack. NASA TN D-5361, 1969.

5. Chambers, Joseph R.; Bowman, James S., Jr.; and Anglin, Ernie L.: Analysis of the Flat-Spin Characteristics of a Twin-Jet Swept-Wing Fighter Airplane. NASA TN D-5409, 1969.

TABLE I.- DIMENSIONAL CHARACTERISTICS OF AIRPLANE

Overall length	57.59 ft (17.55 m)
Wing:	
Span	38.41 ft (11.71 m)
Area (including leading-edge extension)	538.34 ft^2 (50.01 m^2)
Root chord	282.00 in. (716.28 cm)
Tip chord	47.00 in. (119.38 cm)
Mean aerodynamic chord, $\bar{c}$	192.50 in. (488.95 cm)
Leading edge of $\bar{c}$ rearward of leading edge of root chord	110.76 in. (281.33 cm)
Aspect ratio	2.82
Taper ratio	0.167
Sweepback of 25-percent chord	45.00°
Dihedral (inboard 69.5 percent b/2)	0°
Dihedral (outboard 69.5 percent b/2)	12.00°
Incidence	1.00°
Airfoil section:	
Root	NACA 0006.4-64 (modified)
Tip	NACA 0003.0-64 (modified)
Aileron:	
Area (one side) rearward of hinge line	13.08 ft^2 (1.22 m^2)
Span (one aileron) (from 44.5 to 67.0 percent b/2)	4.35 ft (1.33 m) (22.5 percent b/2)
Inboard end chord (base line 103.24 in. (262.23 cm))	37.81 in. (96.04 cm) (21.3 percent $\bar{c}$)
Outboard end chord (base line 155.44 in. (394.82 cm))	34.38 in. (87.33 cm) (27.6 percent $\bar{c}$)
Spoilers:	
Area (one side)	5.44 ft^2 (0.50 m^2)
Span (from 45.3 to 67.0 percent b/2)	4.19 ft (1.28 m)
Inboard end chord	1.39 ft (0.42 m)
Outboard end chord	1.04 ft (0.32 m)
Horizontal tail:	
Area (in chord plane)	94.70 ft^2 (8.80 m^2)
Movable area	77.40 ft^2 (7.19 m^2)
Span	17.705 ft (5.40 m)
Mean aerodynamic chord of horizontal tail	6.143 ft (1.87 m)
Aspect ratio	3.30

TABLE I.- DIMENSIONAL CHARACTERISTICS OF AIRPLANE – Concluded

Taper ratio	0.20
Sweepback of 25-percent chord	35.50°
Dihedral	-23.00°
Root chord (at airplane center line)	107.00 in. (271.78 cm)
Tip chord (theoretical)	21.40 in. (54.36 cm)
Airfoil section:	
Root (airplane center line)	NACA 0003.7-64 (modified)
Tip (theoretical)	NACA 0003.0-64 (modified)
Hinge-line location, percent $\bar{c}_h$	41.00
Vertical tail:	
Area	67.50 ft^2 (6.27 m^2)
Span	6.38 ft (1.94 m)
Taper ratio	0.227
Root chord	207.15 in. (526.16 cm)
Tip chord	47.10 in. (119.63 cm)
Sweepback of 25-percent chord	58.30°
Airfoil section:	
Root	NACA 0004.0-64 (modified)
Tip	NACA 0002.5-64 (modified)
Rudder:	
Area (rearward of hinge line)	11.07 ft^2 (1.03 m^2)
Hinge-line location, percent of water-line chords	80.00

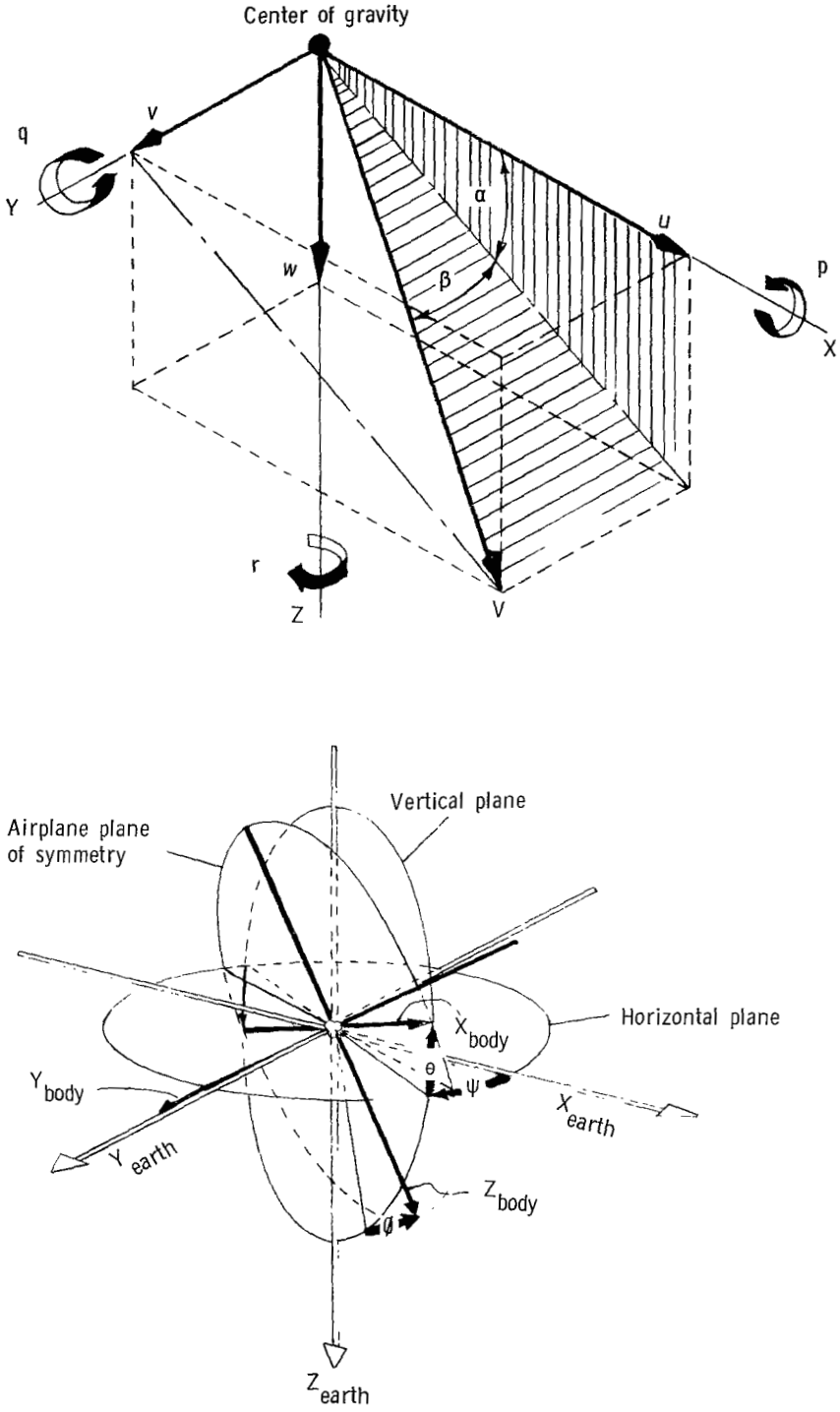

Figure 1.- Body system of axes and related angles.
Arrows indicate positive directions.

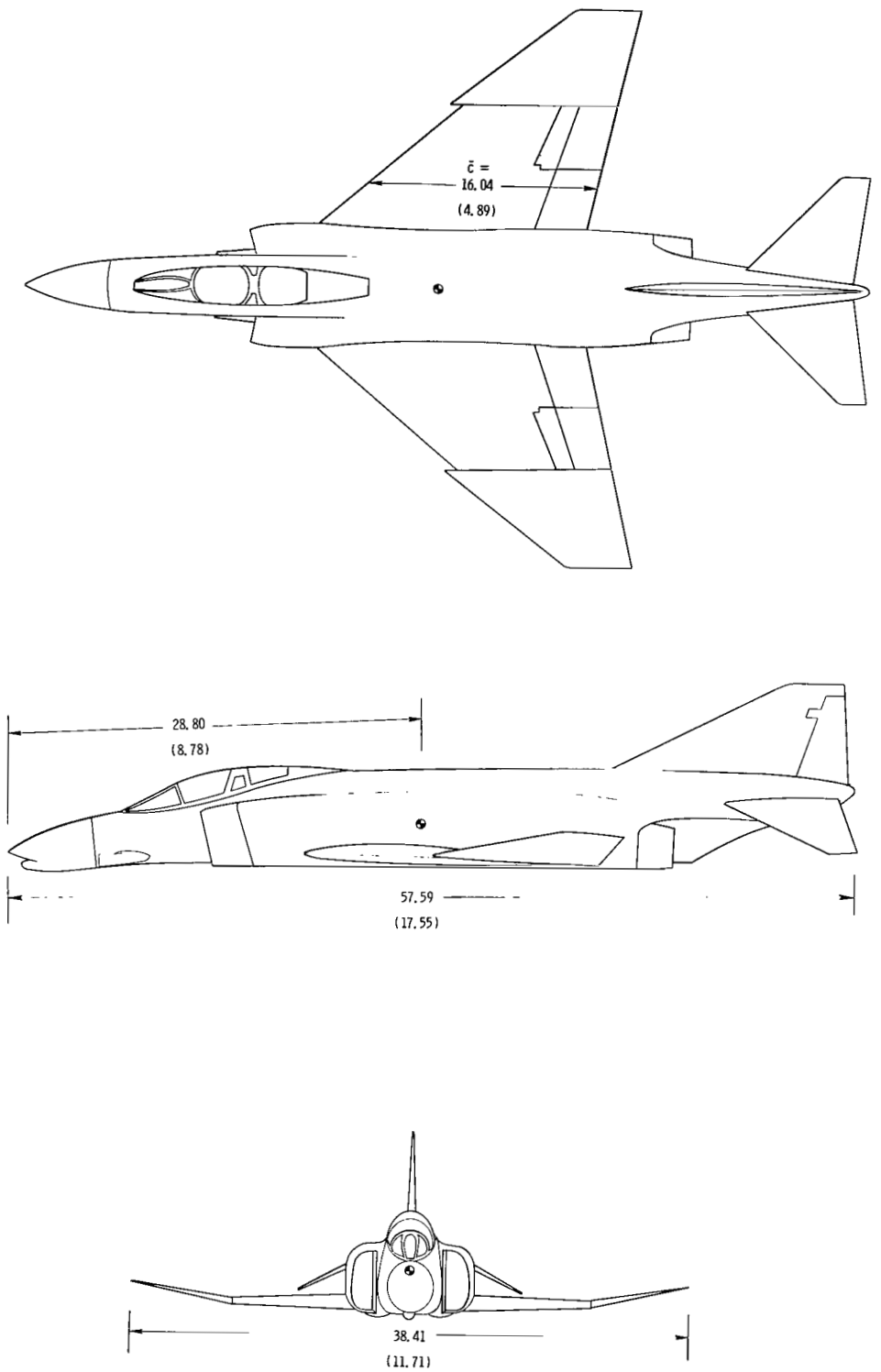

Figure 2.- Three-view sketch of airplane. All dimensions are in feet (meters).

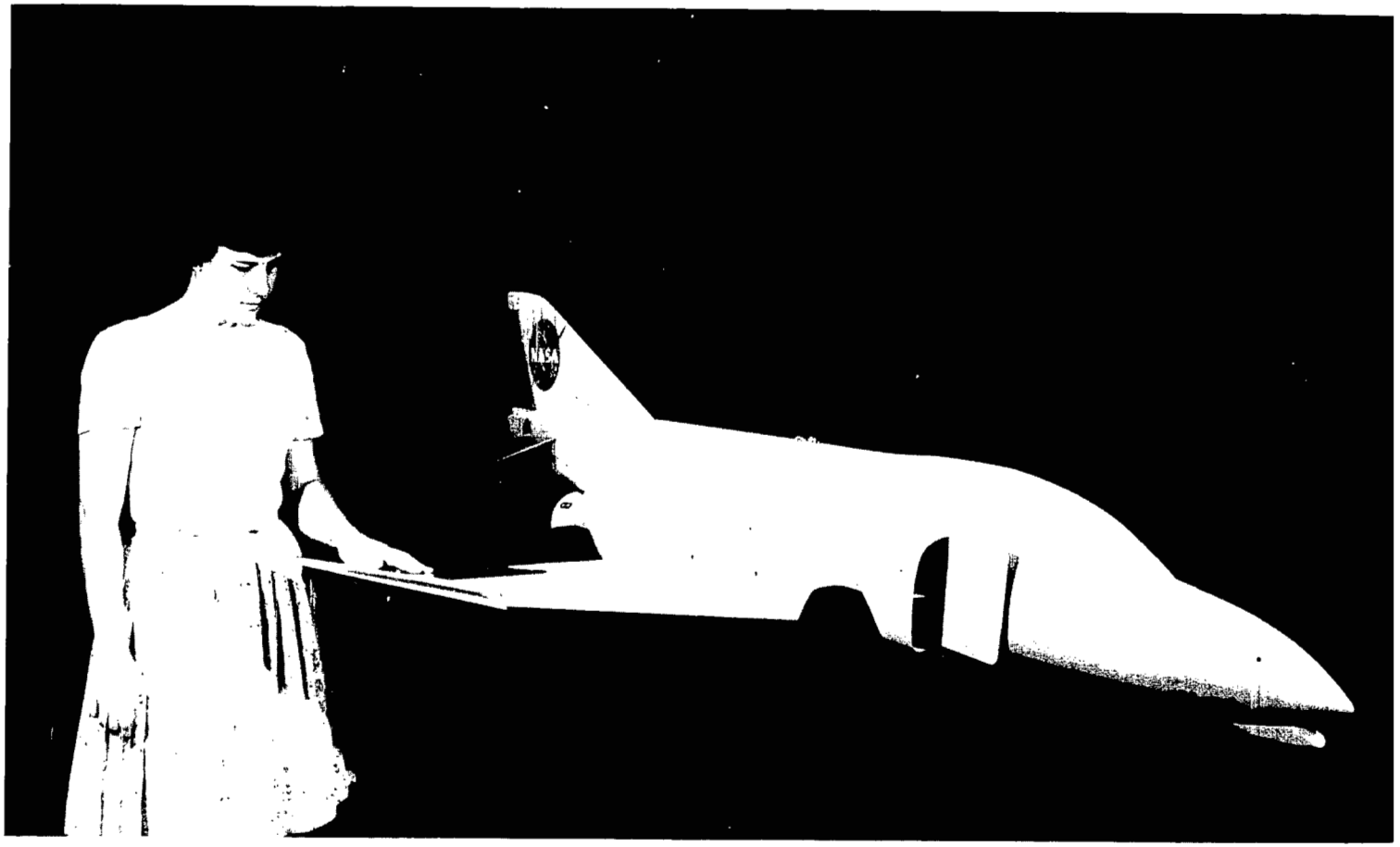

L-70-3313

Figure 3.- Photograph of the 0.13-scale model of the twin-jet fighter airplane.

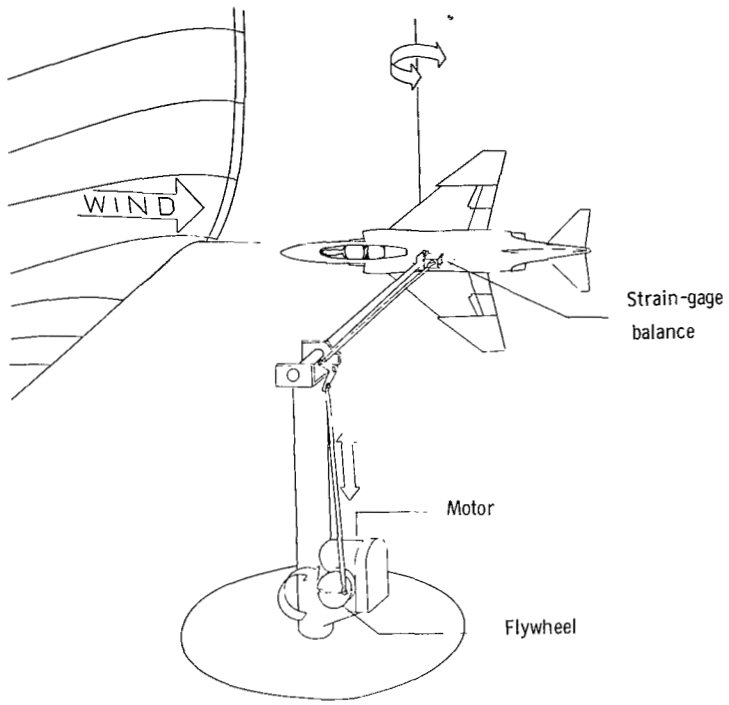

(a) Pitching setup.

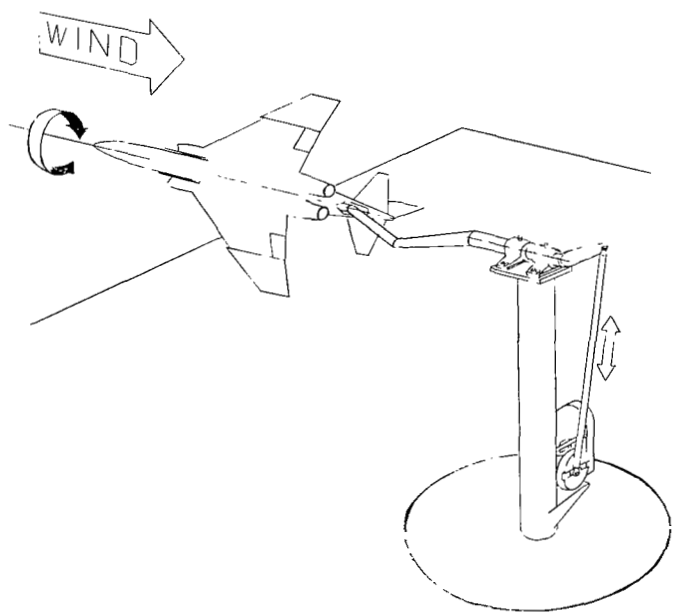

(b) Rolling setup.

Figure 4.- Sketches of test setups for oscillation force tests.

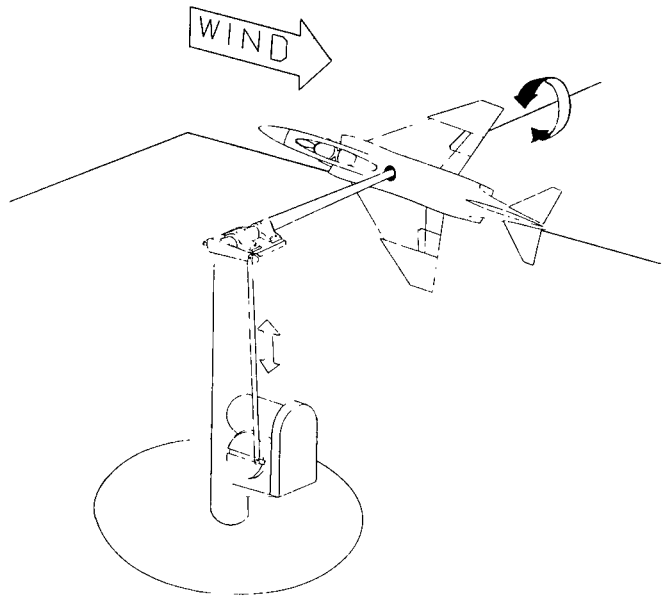

(c) Yawing setup.

Figure 4.- Concluded.

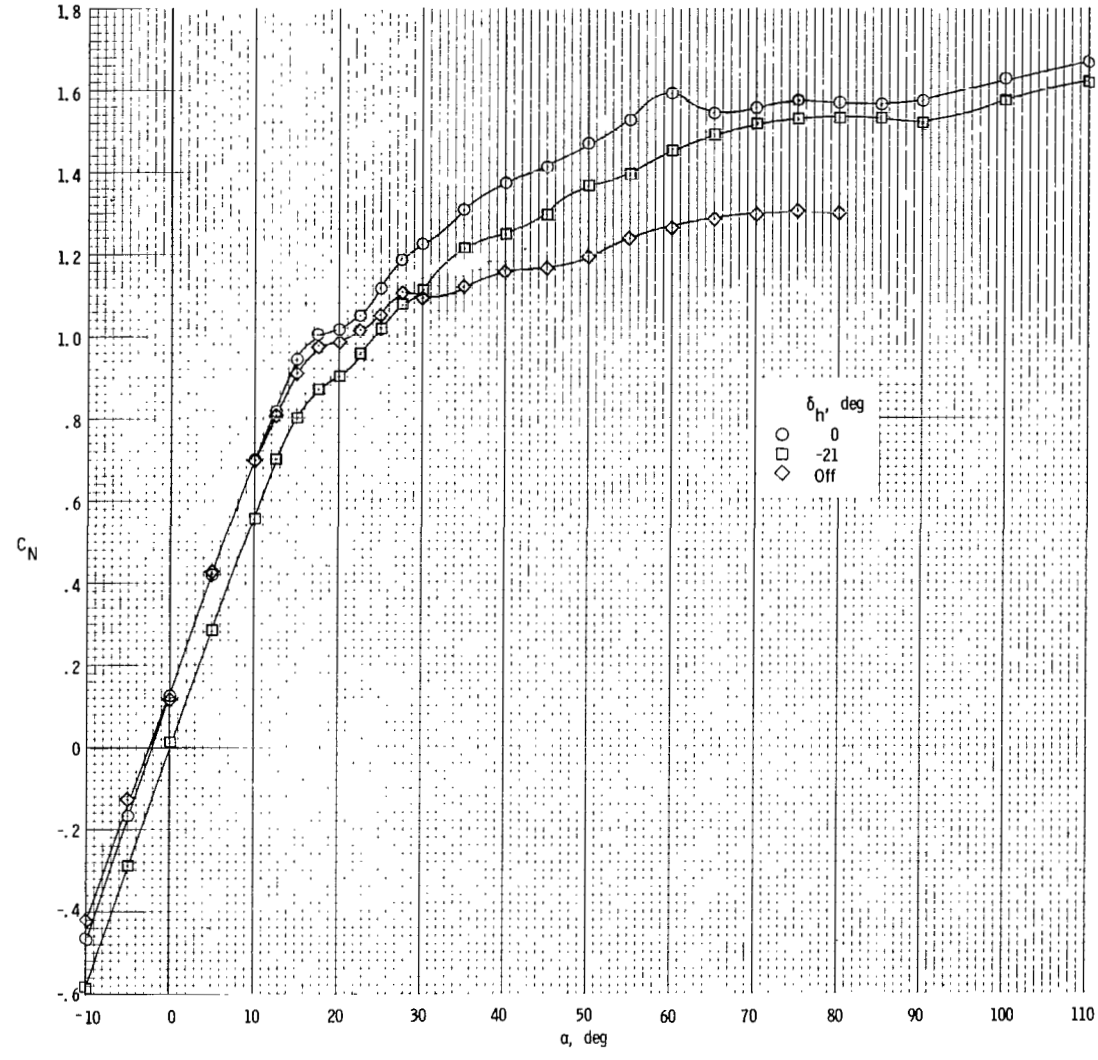

(a) Variation of C_N with α.

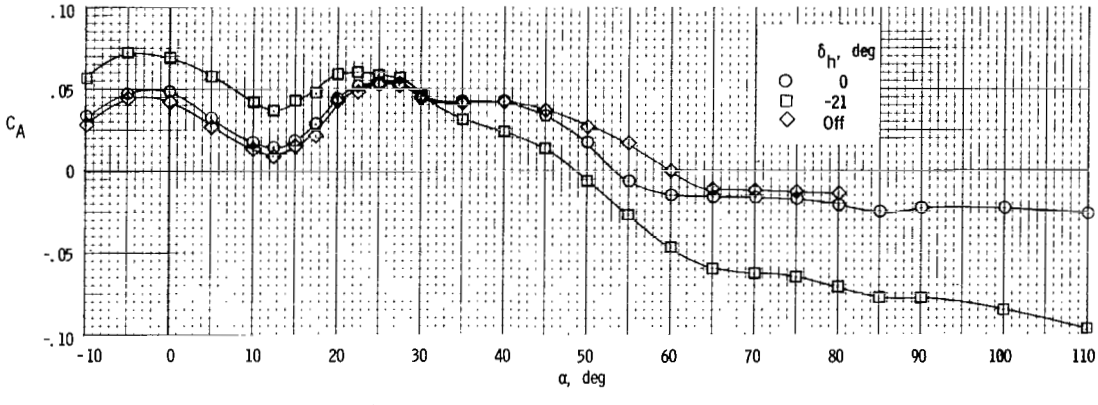

(b) Variation of C_A with α.

Figure 5.- Static longitudinal characteristics of the model. $\beta = 0^o$.

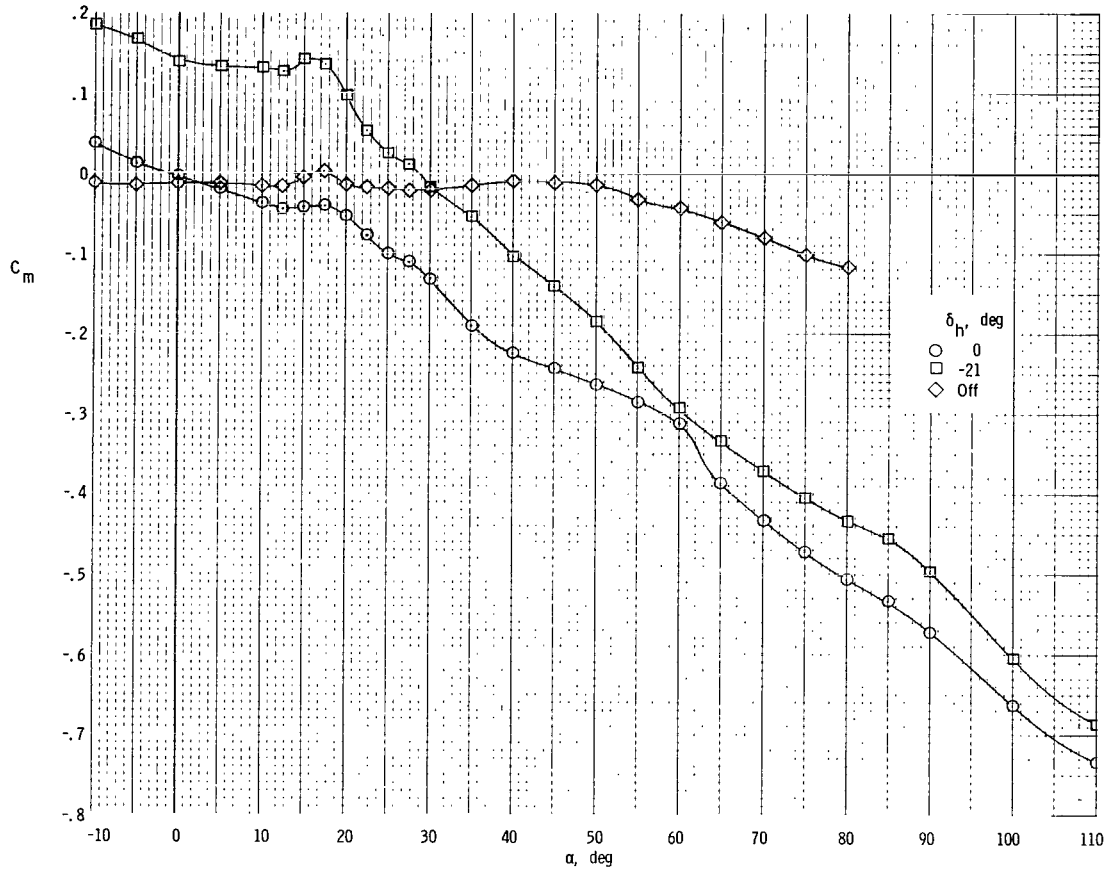

(c) Variation of C_m with α.

Figure 5.- Concluded.

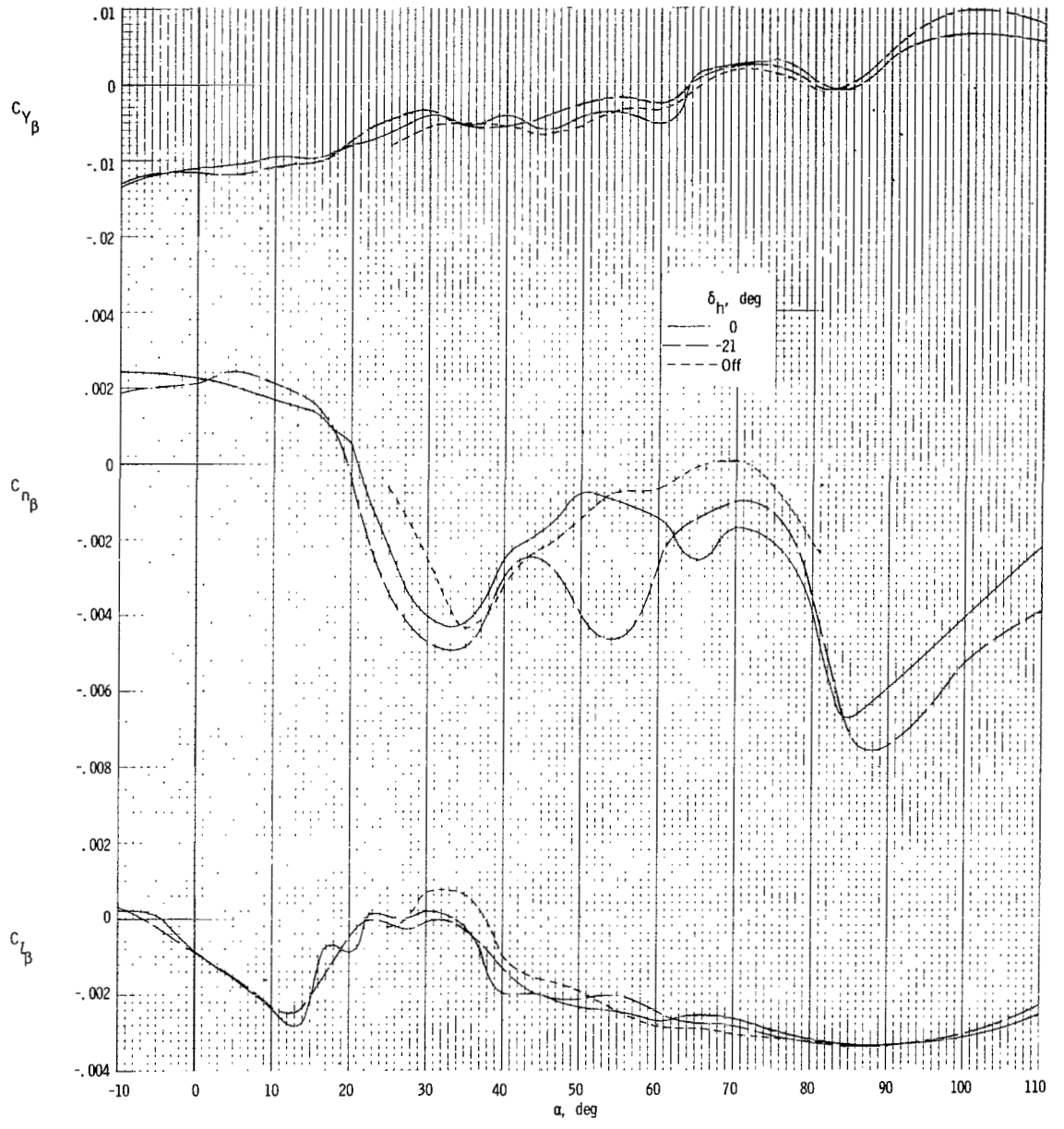

Figure 6.- Static lateral-directional stability derivatives of model.

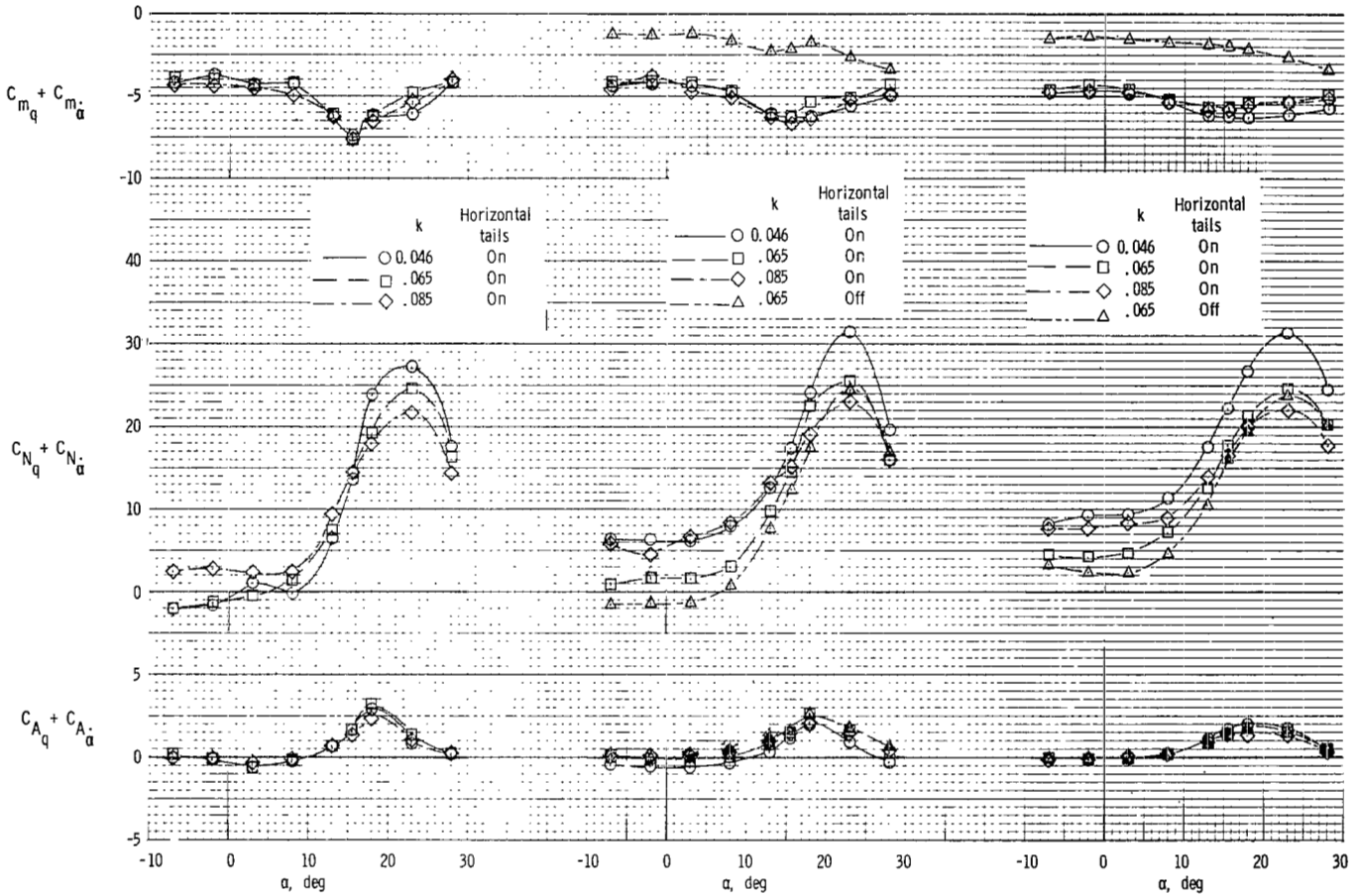

(a) $\Delta\theta = \pm 2.47^{o}$. (b) $\Delta\theta = \pm 4.91^{o}$. (c) $\Delta\theta = \pm 8.16^{o}$.

Figure 7.- Effect of amplitude and frequency and effect of horizontal tails (at one value of frequency only) on the out-of-phase pitching derivatives. $\delta_h = 0^{o}$.

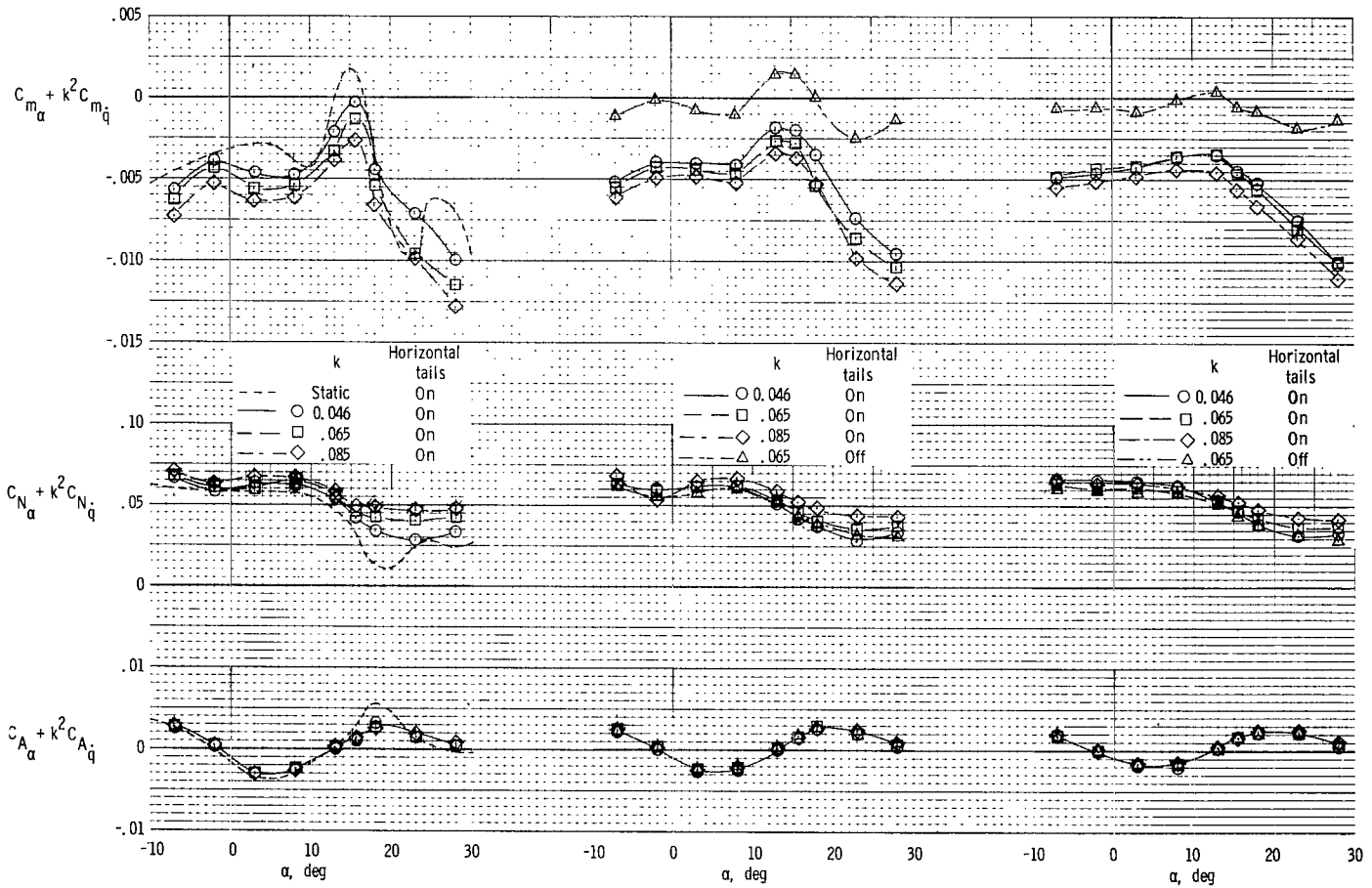

(a) $\Delta\theta = \pm 2.47^{\circ}$. (b) $\Delta\theta = \pm 4.91^{\circ}$. (c) $\Delta\theta = \pm 8.16^{\circ}$.

Figure 8.- Effect of amplitude and frequency and the effect of horizontal tails (at one value of frequency only) on the in-phase pitching derivatives. $\delta_h = 0^{\circ}$.

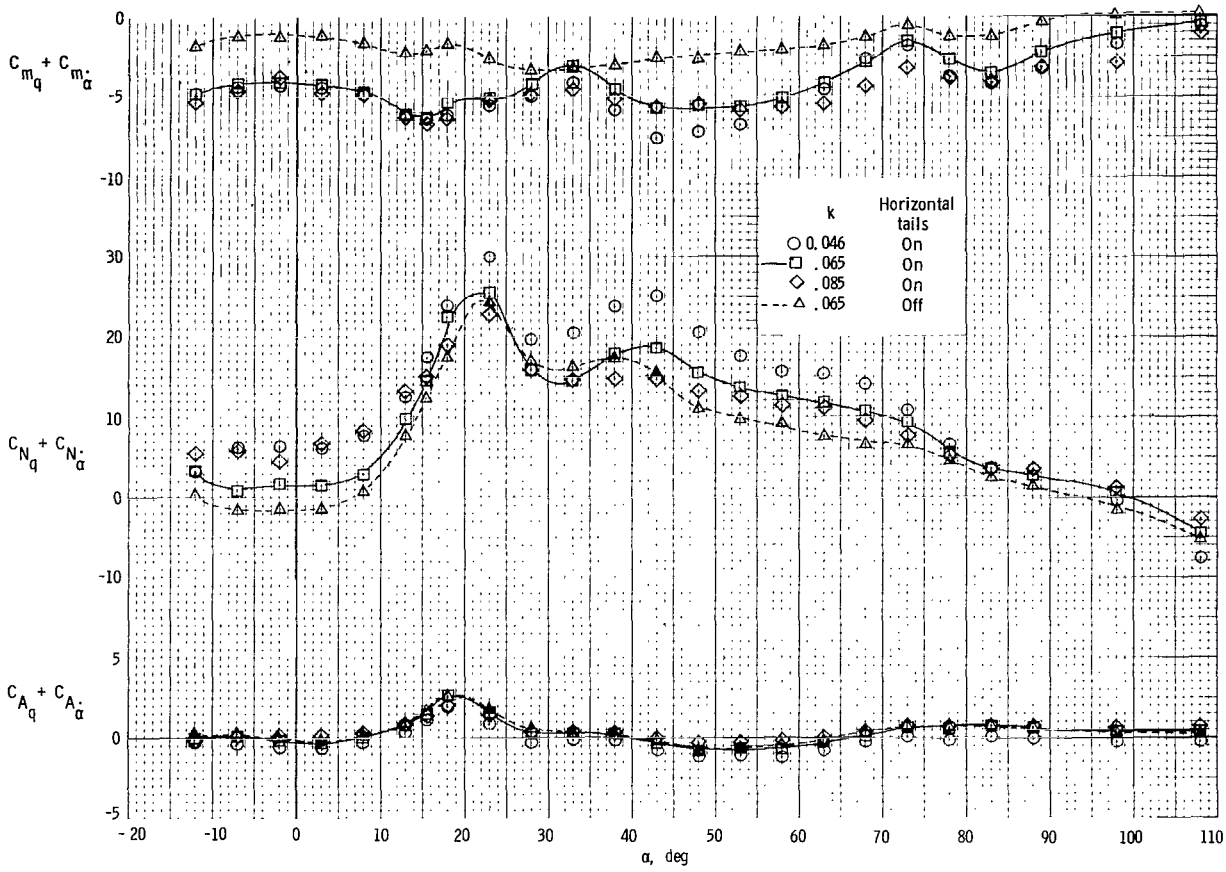

(a) $\Delta\theta = \pm 4.91^{\circ}$.

Figure 9.- Effect of frequency and horizontal tails on out-of-phase pitching derivatives. $\delta_h = 0^{\circ}$.

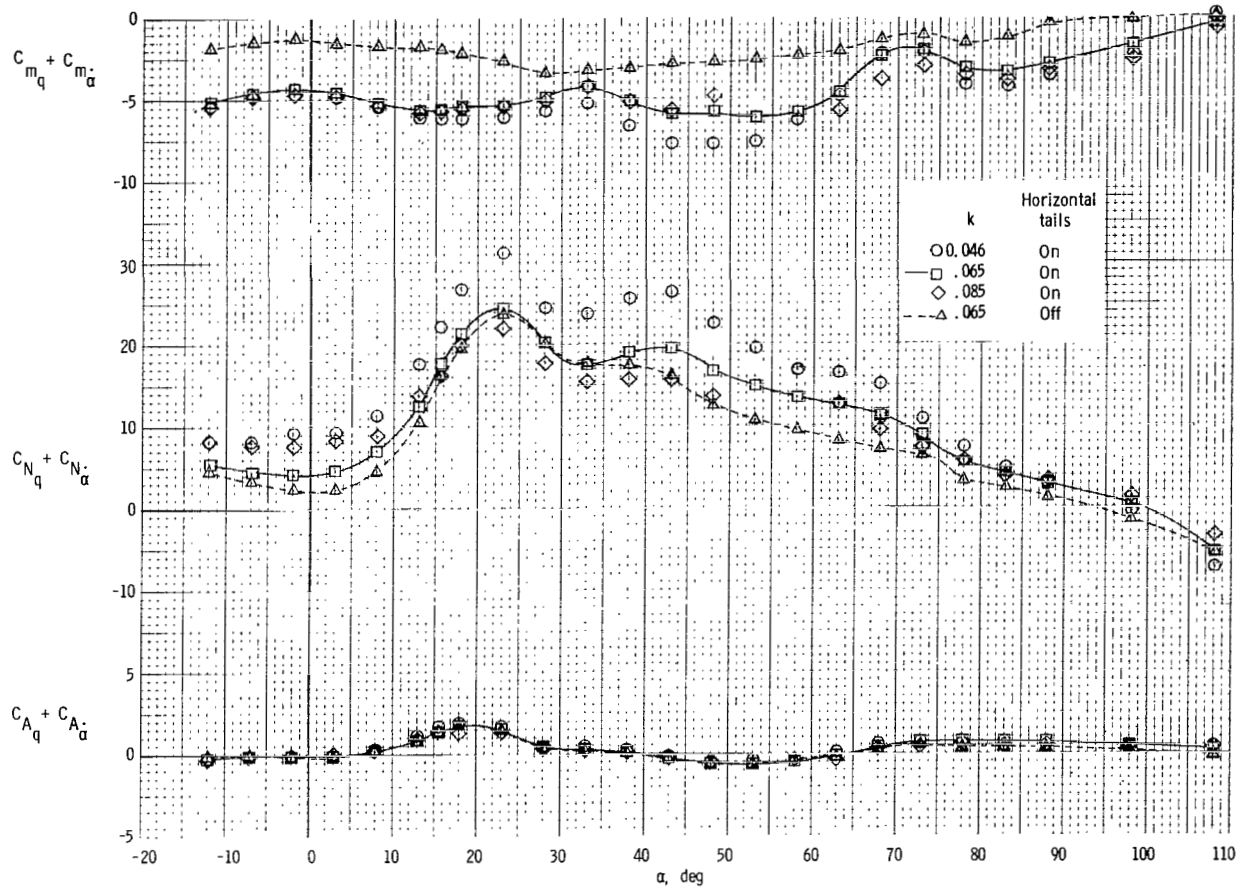

(b) $\Delta\theta = \pm 8.16^{\circ}$.

Figure 9.- Concluded.

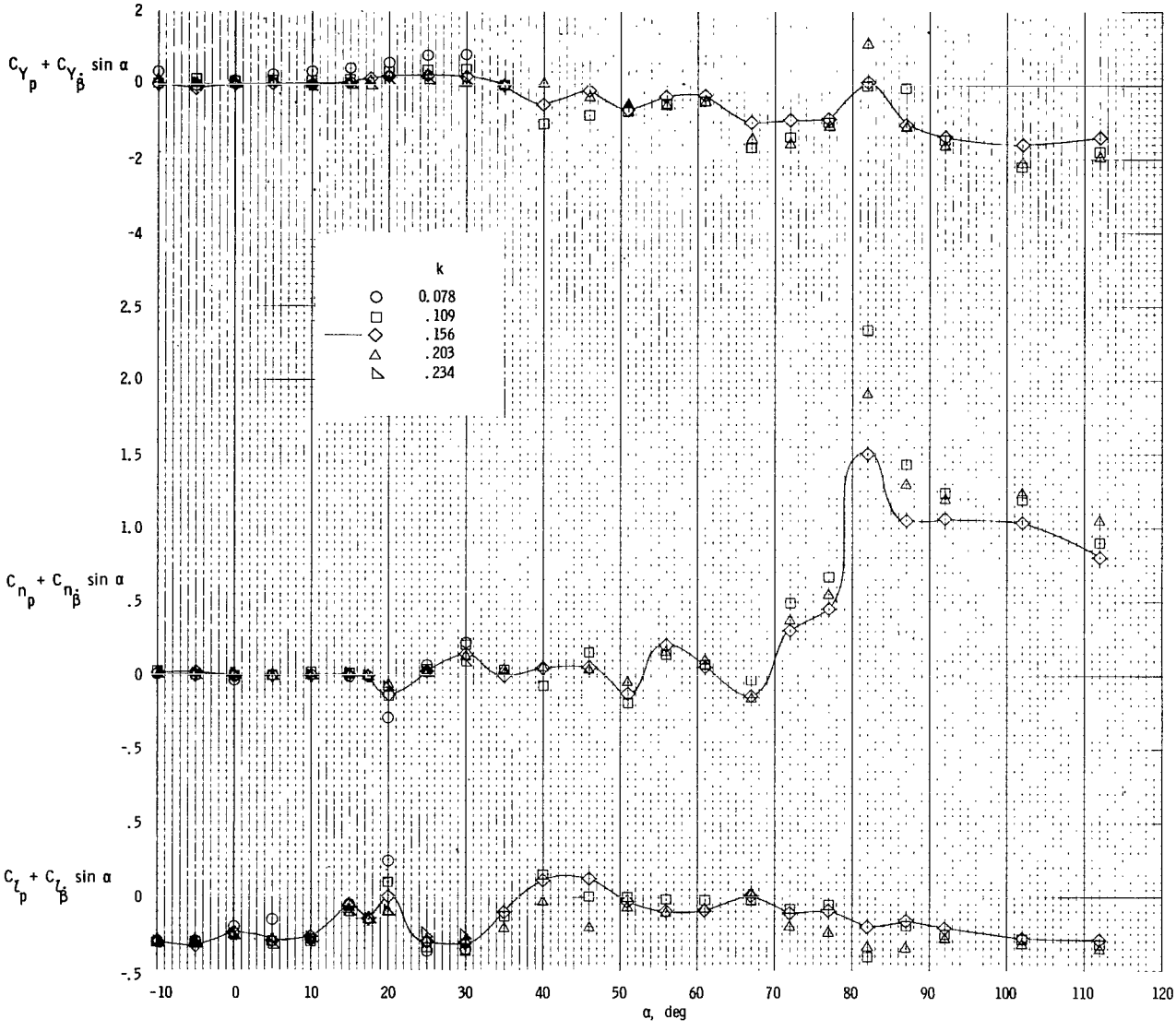

(a) $\Delta\phi = \pm 5.00^{o}$.

Figure 10.- Effect of frequency and amplitude on the out-of-phase rolling derivatives. $\delta_h = 0^{o}$.

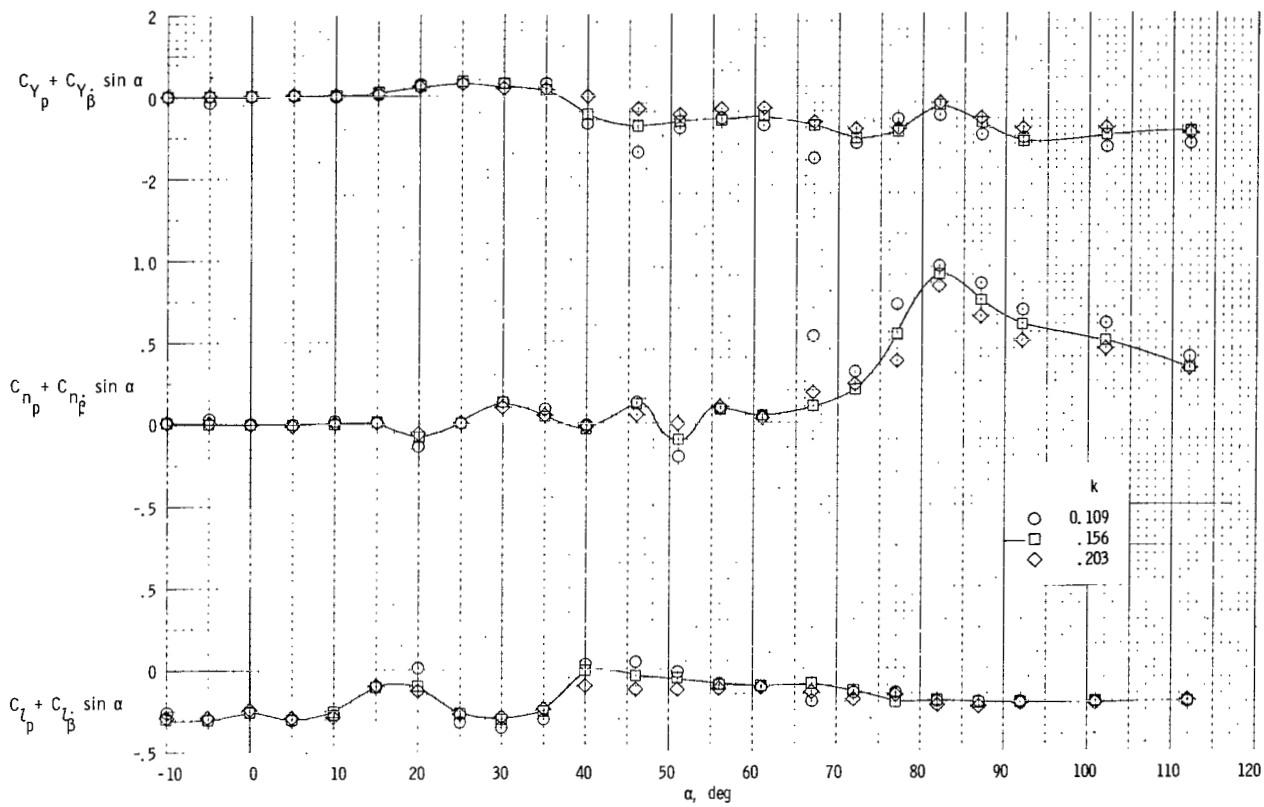

(b) $\Delta\phi = \pm 10.50^{o}$.

Figure 10.- Concluded.

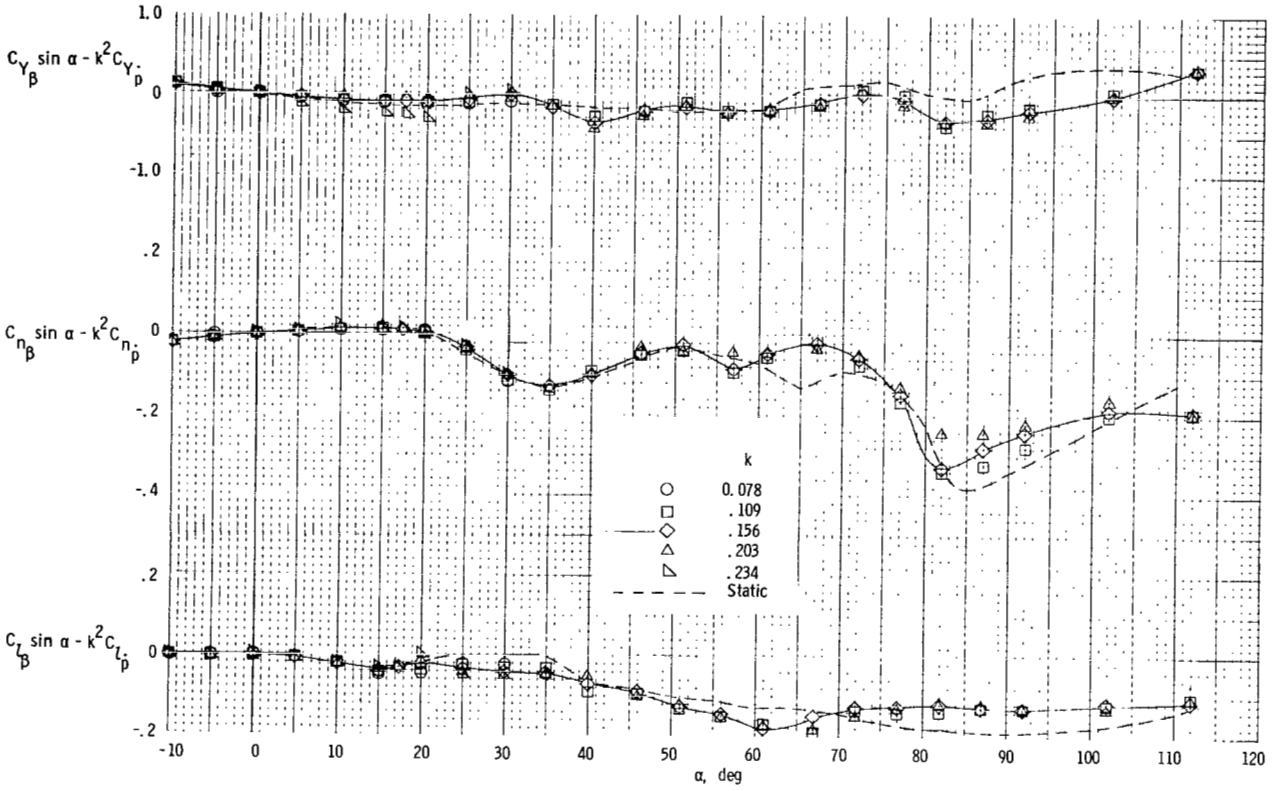

(a) $\Delta\phi = \pm 5.00^{o}$.

Figure 11.- Effect of frequency and amplitude on the in-phase rolling derivatives. $\delta_h = 0^{o}$.

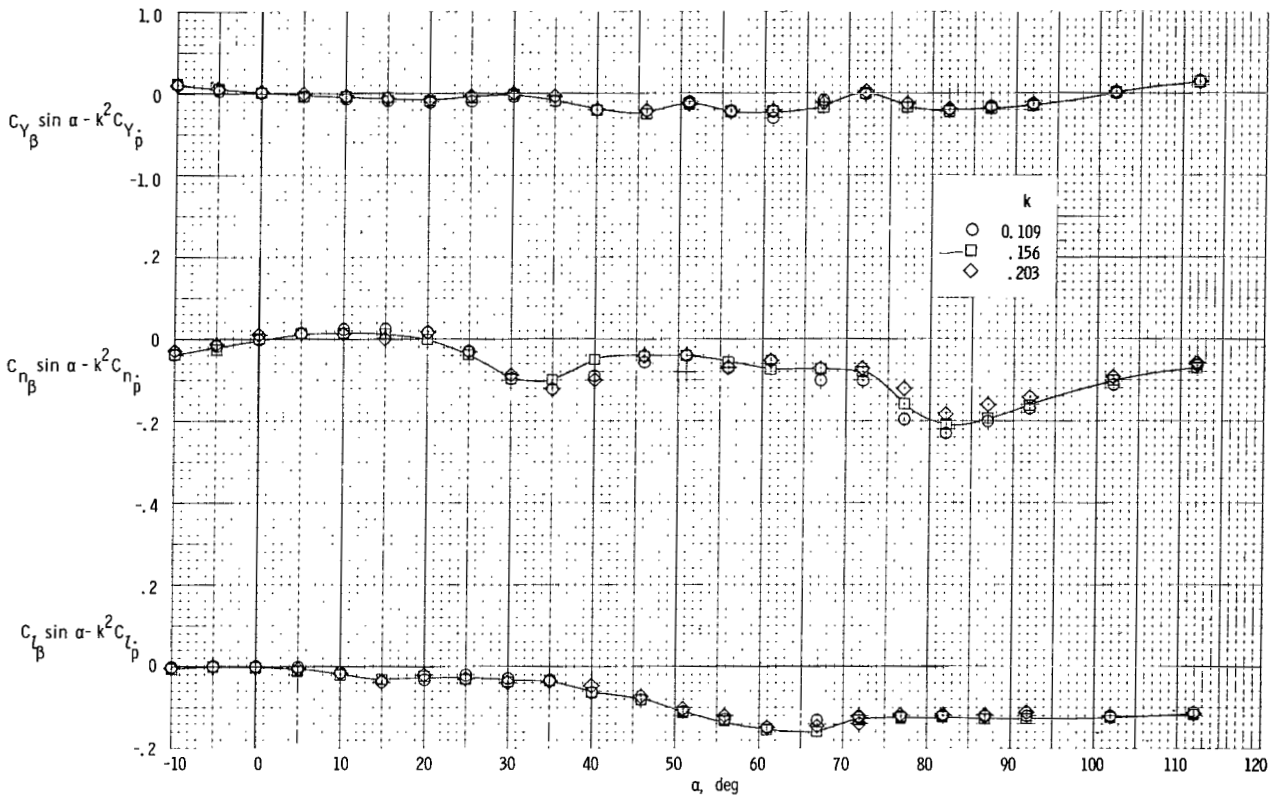

(b) $\Delta\phi = \pm 10.50^{o}$.

Figure 11.- Concluded.

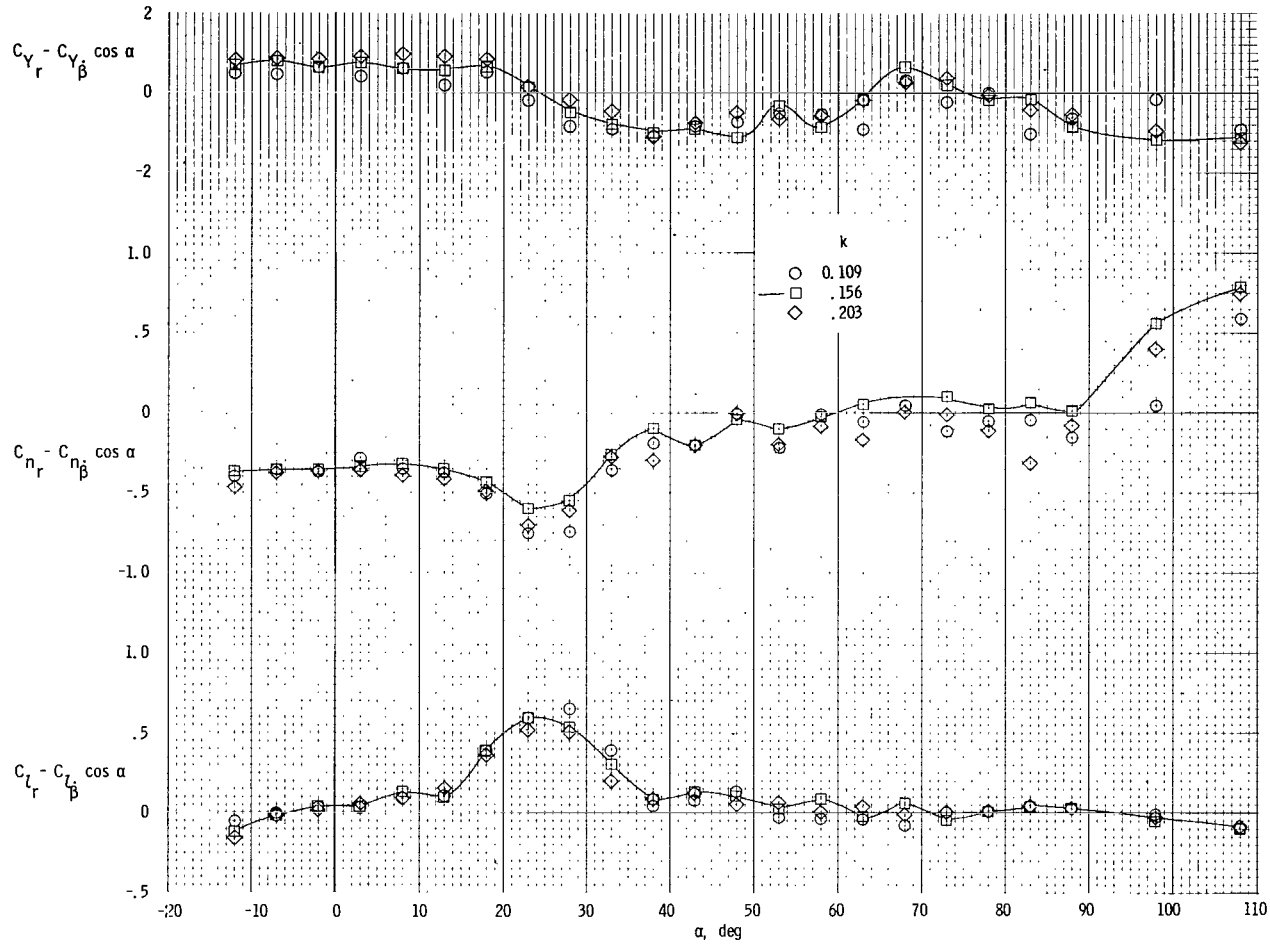

(a) $\Delta\psi = 5.25^{o}$.

Figure 12.- Effect of frequency and amplitude on out-of-phase yawing derivatives. $\delta_h = 0^{o}$.

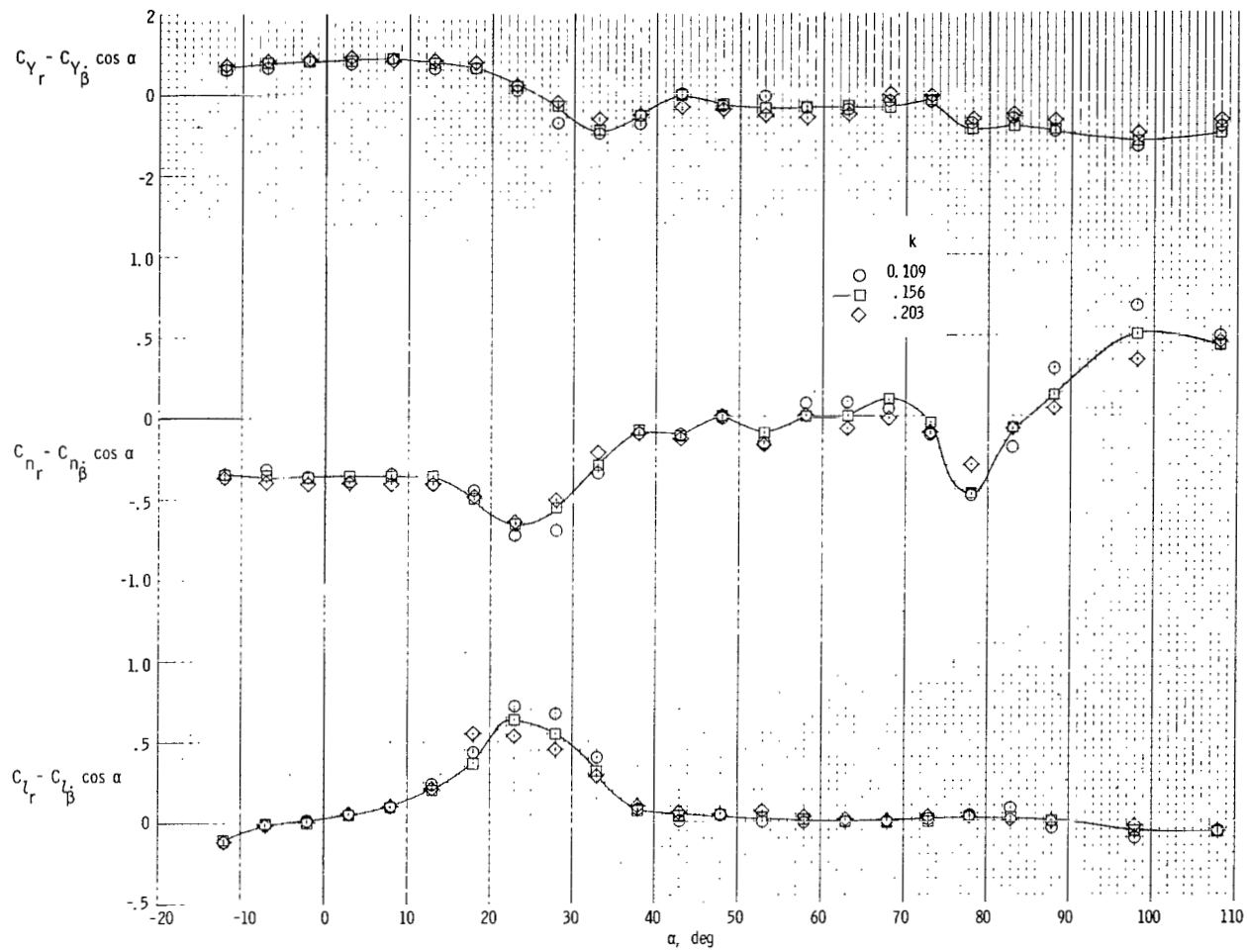

(b) $\Delta\psi = 10.50^{o}$.

Figure 12.- Concluded.

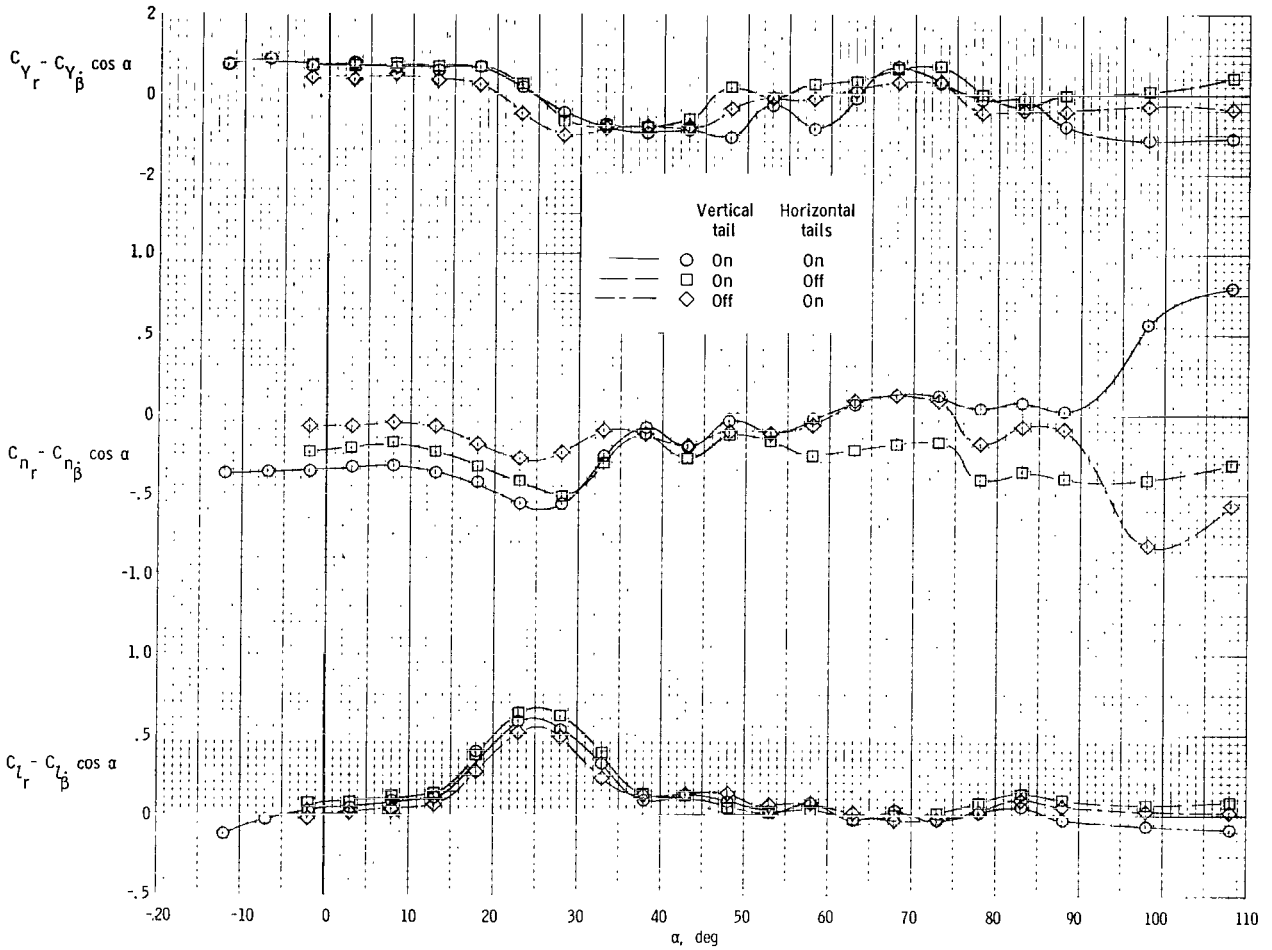

(a) Out-of-phase derivatives.

Figure 13.- Effect of vertical and horizontal tails on the yaw oscillation derivatives. $\Delta\psi = \pm 5.25^{o}$; k = 0.156.

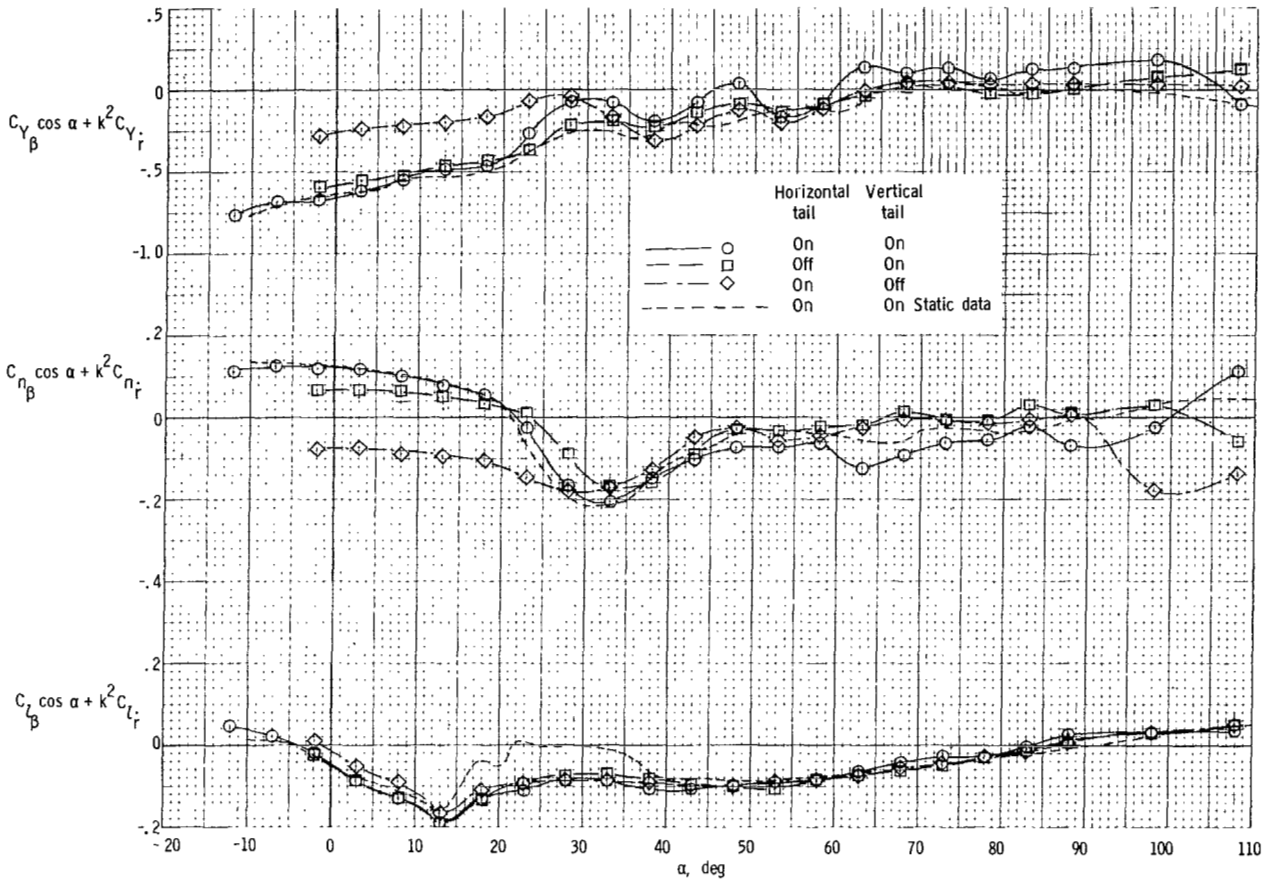

(b) In-phase derivatives.

Figure 13.- Concluded.

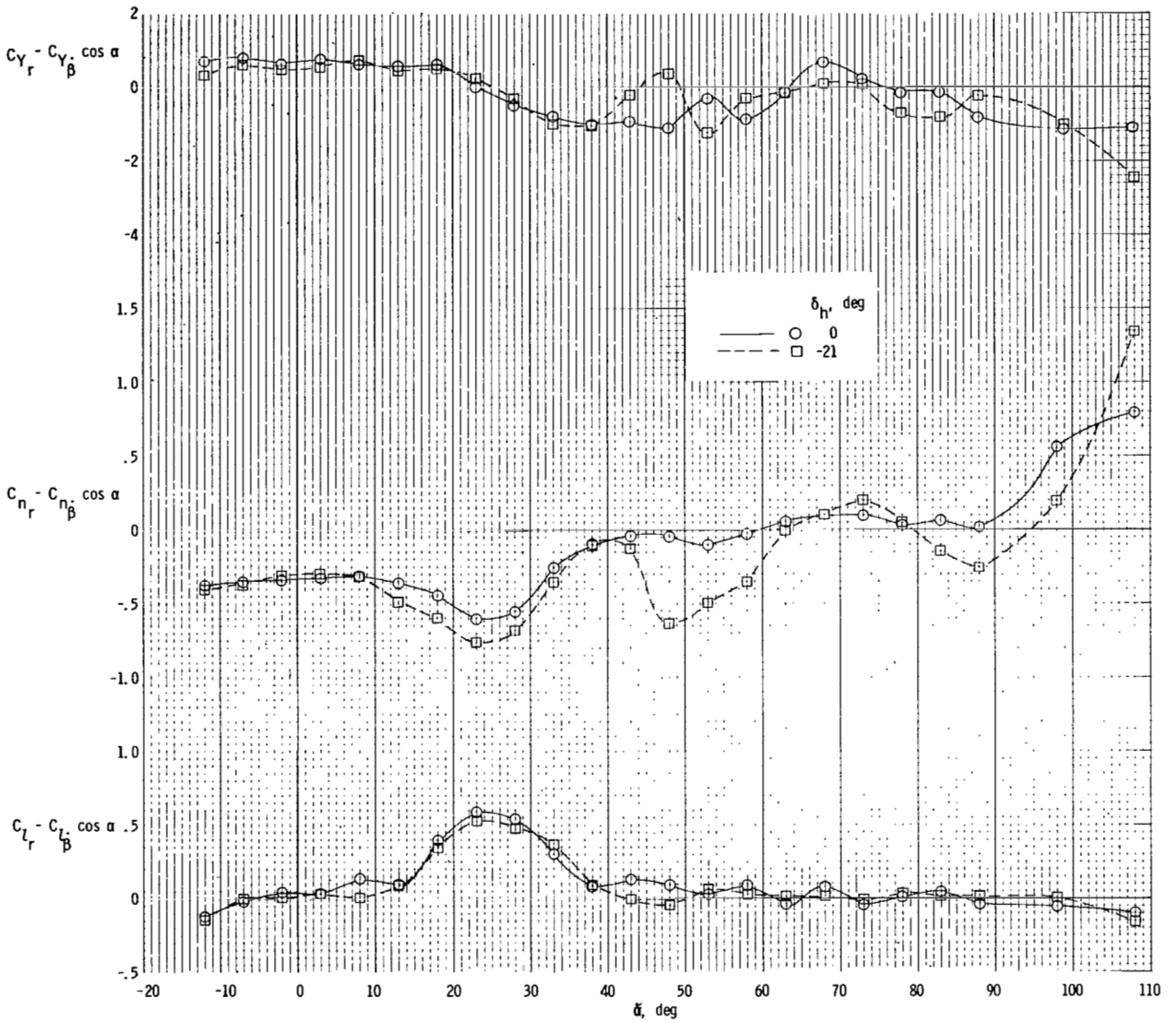

(a) Out-of-phase derivatives.

Figure 14.- Effect of horizontal-tail deflection on the yawing oscillation derivatives. $\Delta\psi = \pm 5.25^{o}$; k = 0.156.

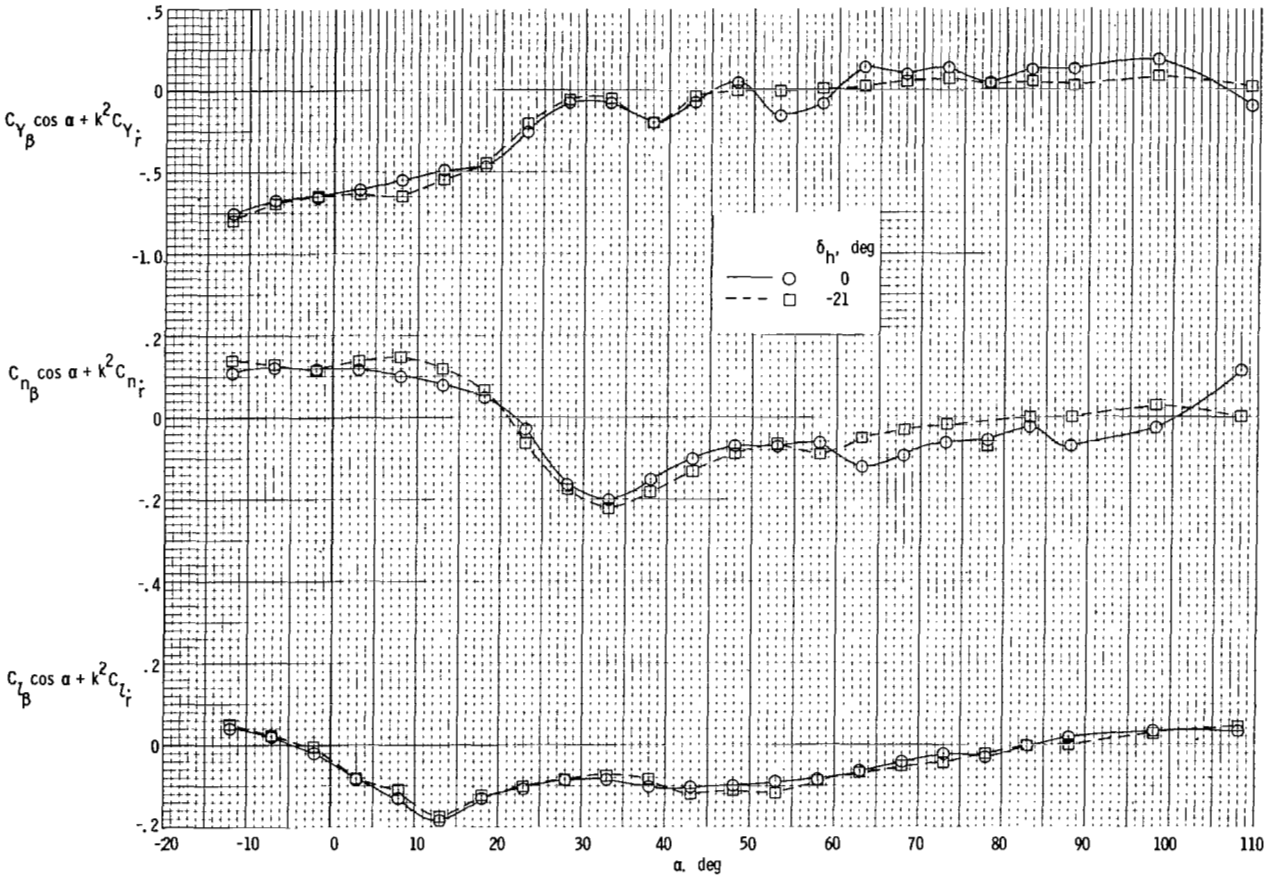

(b) In-phase derivatives.

Figure 14.- Concluded.

"The aeronautical and space activities of the United States shall be conducted so as to contribute . . . to the expansion of human knowledge of phenomena in the atmosphere and space. The Administration shall provide for the widest practicable and appropriate dissemination of information concerning its activities and the results thereof."

—NATIONAL AERONAUTICS AND SPACE ACT OF 1958

NASA SCIENTIFIC AND TECHNICAL PUBLICATIONS

TECHNICAL REPORTS: Scientific and technical information considered important, complete, and a lasting contribution to existing knowledge.

TECHNICAL NOTES: Information less broad in scope but nevertheless of importance as a contribution to existing knowledge.

TECHNICAL MEMORANDUMS: Information receiving limited distribution because of preliminary data, security classification, or other reasons.

CONTRACTOR REPORTS: Scientific and technical information generated under a NASA contract or grant and considered an important contribution to existing knowledge.

TECHNICAL TRANSLATIONS: Information published in a foreign language considered to merit NASA distribution in English.

SPECIAL PUBLICATIONS: Information derived from or of value to NASA activities. Publications include conference proceedings, monographs, data compilations, handbooks, sourcebooks, and special bibliographies.

TECHNOLOGY UTILIZATION PUBLICATIONS: Information on technology used by NASA that may be of particular interest in commercial and other non-aerospace applications. Publications include Tech Briefs, Technology Utilization Reports and Technology Surveys.

Details on the availability of these publications may be obtained from:

SCIENTIFIC AND TECHNICAL INFORMATION OFFICE

NATIONAL AERONAUTICS AND SPACE ADMINISTRATION

Washington, D.C. 20546